Copyright © 2008 American Scientific Publishers
All rights reserved
Printed in the United States of America

Journal of
Nanoscience and Nanotechnology
Vol. 8, 2836–2857, 2008

REVIEW

Superparamagnetism and Other Magnetic Features in Granular Materials: A Review on Ideal and Real Systems

M. Knobel[1,*], W. C. Nunes[1], L. M. Socolovsky[2], E. De Biasi[3], J. M. Vargas[4], and J. C. Denardin[5]

[1] *Instituto de Física 'Gleb Wataghin,' Universidade Estadual de Campinas CP 6165, 13083-970 Campinas (SP), Brazil*
[2] *Instituto de Física, Universidade Federal de Goiás, Campus Samambaia, 74001-970 Goiânia (GO), Brazil*
[3] *Laboratório Nacional de Luz Síncrotron, Av. Giuseppe M. Scolfaro 10000, 13084-971 Campinas (SP), Brazil*
[4] *Centro Atomico Bariloche & Instituto Balseiro, CP 8400, S. C. Bariloche, Rio Negro, Argentina*
[5] *Departamento de Física, Universidad de Santiago de Chile, USACH, Santiago, Chile*

An overview on magnetic of nanostructured magnetic materials is presented, with particular emphasis on the basic features displayed by granular nanomagnetic solids. Besides a review of the basic concepts and experimental techniques, the role of structural disorder (mainly the distribution of grain sizes), interparticle magnetic interactions and surface effects are also discussed with some detail. Recent results, models and trends on the area are also discussed.

Delivered by Ingenta to:
Boulder Labs Library
IP : 132.163.130.245
Mon, 11 Aug 2008 15:50:43

Keywords: Nanocrystalline Solids, Nanomagnetism, Superparamagnetism, Dipolar Interactions, Magnetism.

CONTENTS

1. Introduction 2836
2. Superparamagnetism: Brief Introduction 2838
3. Nanoparticle Ensembles 2840
3.1. Langevin Equation 2840
3.2. Initial Magnetic Susceptibility 2841
3.3. Grain Size Distribution and Measurement Techniques 2841
3.4. Typical Measurements for Magnetic Characterization of Granular Systems: ZFC and FC Magnetization Curves . . . 2842
3.5. TRM Curves 2844
3.6. Log-Normal Size Distribution 2844
3.7. Coercive Field 2845
3.8. Time Relaxation 2847
4. Interacting Superparamagnetic Systems 2848
4.1. Interacting Superparamagnetic Model 2849
4.2. Effect of Interactions on the Blocking Temperature 2851
5. The Role of the Surface 2853
6. Conclusions 2854
Acknowledgments 2854
References and Notes 2854

1. INTRODUCTION

Nanoscopic magnetic systems are composed by magnetic particles or agglomerates with at least one dimension with characteristic size of the order of nanometers. One can find systems with nanometric particles distributed in solids (also known as granular solids), or liquids (also called magnetic fluids or ferrofluids). In the case of granular solids, the matrix in which the nanoparticles are immersed can be an electric insulator or a conductor, crystalline or amorphous; and can have several phases of different materials. Therefore, physical properties of the nanoparticulated systems can be tailored for specific purposes in academic or technological research. One can easily highlight the use of nanoparticles to obtain enhanced hard magnets, soft magnetic materials with lower energy losses and rapid magnetic response at variable magnetic fields, magnetic microsensors, and a myriad of applications, as in medical diagnosis, catalysis, magnetic liquids for drug delivery, pigments for painting and ceramics, among others.[1,2] One can also naturally find magnetic nanoparticles in some animals or bacteria.[3–6] Furthermore, the huge impulse that research in nanostructured magnetic systems has received in the last years comes from the enormous prospectives of their use in magnetic recording technology, either in the design of better recording heads or in the development of high density magnetic media, which would use the direction of the magnetic moments of the individual nanoparticles arranged in a disk surface.[7]

Ultrafine solid particles can be prepared by means of several methods, such as chemical reduction, colloidal routes, vapor deposition, sputtering, melt-spinning, electrodeposition, mechanical alloying.[1,2,8] The final nanostructure can be tailored by further annealing, either in

*Author to whom correspondence should be addressed.

1533-4880/2008/8/2836/022 doi:10.1166/jnn.2008.017

Marcelo Knobel is an Associate Professor of the Instituto de Física "Gleb Wataghin" (Gleb Wataghin Physics Institute), of the Universidade Estadual de Campinas (State University of Campinas, UNICAMP). He has a Ph.D. in Physics from UNICAMP, and post-doctorate stages at "Istituto Elettrotecnico Nazionale Galileo Ferraris," Turin, Italy, and "Instituto de Magnetismo Aplicado," Madrid, Spain. Since 1999 he leads the Laboratório de Materiais e Baixas Temperaturas (Materials and Low Temperatures Laboratory). Knobel has published more than 200 articles in refereed journals, mainly in the field of magnetism and magnetic materials. Within this field, his interests are in basic and applied properties of artificially grown amorphous and nanocrystalline systems. Dr. Knobel has been enthusiastically promoting the popularization of science and technology in Brazil.

Wallace C. Nunes is an Assistant Professor of Condensed Matter Physics Centre at University of Lisbon since March 2008. He worked with Professor M. A. Novak on magnetic properties of nanoparticles and molecular based materials and received his Ph.D. in 2003 from Universidade Federal do Rio de Janeiro. From 2003 to 2007, he worked as Post-doc at UNICAMP. His research interest include experiment and analysis of nanostructured magnetic systems, development of phenomelogical models, especially in superparamagnetism, spin glasses and reentrant spin glass properties.

Delivered by Ingenta to:
Boulder Labs Library
IP : 132.163.130.249
Mon, 11 Aug 2008 19:50:43

Leandro M. Socolovsky earned his Ph.D. at Universidad Nacional de La Plata (Argentina). He held positions as a post-doc at Universidade Estadual de Campinas and Universidade Federal de Goiás (Brazil). Now he is a staff researcher of the INTECIN, at the Facultad de Ingeniería, Universidad de Buenos Aires, Buenos Aires (Argentina).

ASP
AMERICAN SCIENTIFIC PUBLISHERS

Emilio De Biasi was born in Villa Dolores, Córdoba, Argentina in 1973, received his Ph.D. degree in Physics in 2005 at Instituto Balseiro, Argentina. He is an Assistant Researcher of CONICET at Centro Atómico Bariloche, Bariloche, Argentina.

José M. Vargas was born in Argentina. He studied Physics at Balseiro Institute-Cuyo University (IB-CAB, Argentina), where he obtained his B.Sc. degree in 2001. He continued his studies at UNICAMP (Brazil) where he obtained the M.Sc. degree in 2004. He carried out his doctoral studies Balseiro Institute-Cuyo University, Argentina, finishing it in 2007. His main research interests lie in the finite size and cristalline field effects on the magnetic properties in model nanostructured systems of transition metal and rare-earth compounds, which include organic functionalization of particle surfaces.

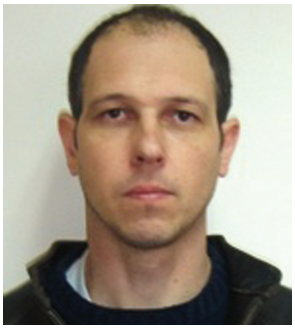

Juliano Casagrande Denardin was born in Santa Maria, Brazil, in 1971, received his Ph.D. degree in Physics in 2002 at UNICAMP, Brazil. Since 2005 he is an Assistant Professor at Universidad de Santiago, Chile. He is also researcher of the Millennium Science Nucleus Basic and Applied Magnetism P06-022F.

REVIEW

conventional ovens or by Joule heating.[9, 10] The nanostructured systems that are thus created display a broad variety of interesting physical properties, which, together with their technological relevance, make them a unique set for studying a diversity of interesting problems in solid state physics, such as superparamagnetism;[11–13] grain nucleation and growth kinetics,[14, 15] spin glass behavior,[16, 17] exchange bias,[18–20] competition between different magnetic energies.[21–29] Also, the interest in magnetic granular systems was reinforced by the discovery of giant magnetoresistance (GMR) in artificially grown layered structures.[30] The field of magnetotransport phenomena has been continuosly growing, and some metal-insulator composites have shown interesting magnetotransport properties such as tunnel magnetoresistance (TMR),[31] or giant Hall Effect (GHE).[32]

In order to design better materials for specific applications, it is fundamental to understand the intrinsic but intricate relationship between the macroscopic magnetic properties and nanostructural features. However, most frequently the nanoscopic systems are composed by crystallites randomly dispersed within a matrix, with a rather large dispersion of grain sizes and interparticle distances. Furthermore, the lack of homogeneity of the nanocrystals (both in shape and composition), allied with the unavoidable magnetic interactions among the magnetic entities, usually complicate the analysis and interpretation of the observed magnetic properties.[1, 33, 34] In an effort to better understand these complex issues several groups started to synthetize magnetic nanoparticles by means of chemical methods, which allows one to obtain rather narrow particle size distributions. As an advantage over other fabrication procedures, such methods usually provide a coating of the nanoparticles that prevents the direct contact among nanoparticles, leading to novel samples with interesting properties. By using Langmuir-Blodgett techniques some groups obtained organized arrays of nanoparticles.[35–39] Such samples rule out the complications introduced by positional randomness and therefore they provide an excellent platform to study the dynamics of the magnetization of a collective behavior caused by magnetic interactions.[40] It is worth mentioning that magnetic interactions indeed play an important role in the magnetic behaviour of these systems. In fact, the specific collective state induced by the interactions in a given system depends on its structural features—mainly concentration of particles and their geometrical and size distribution—and on the nature of the matrix (metallic or insulating). In the case of granular systems with essentially dipolar interactions, there are evidences that small closed-flux structures can appear, leading to a sort of superferromagnetic state.[11, 41] It is possible, in some specific cases, to obtain phenomenological expressions relating individual and collective properties of interacting nanomagnetic systems.

In this review we present a brief introduction to the phenomenology of superparamagnetism. We discuss few fundamental concepts, starting from the expected properties of a single particle. Thus, the expected behavior of non-interacting nanoparticle ensembles, considering real size distributions. The role of dipolar magnetic interactions and surface effects will also be discussed. An outline of the current research on granular magnetic systems will be given, with a brief revision of the basic theories, and some illustrative examples that have been studied by our research group.

2. SUPERPARAMAGNETISM: BRIEF INTRODUCTION

Attempts to produce tiny dispersions of magnetic materials in metals have been done since the 1930s.[42, 43] Apparently, the first modelization of a nanometered-size particle was done by Kittel in 1946.[44] From the very beginning, the models considered that the magnetic moment would follow an Arrhenius law, with a characteristic relaxation time τ, as will be described below. Nevertheless, the determination of τ was only solved by Néel,[45] in 1949. He supposed that each nanoparticle was formed by rigidly aligned spins that rotate coherently during magnetization reversal, considering the case of uniaxial anisotropy when the energy barrier is much larger than the thermal energy of the system. The equivalence with a gyroscopic system allowed him to derive an expression for τ, as a function of gyromagnetic ratio, longitudinal magnetostriction constant, Young modulus, energy barrier and thermal energy. He estimated characteristic time relaxation to be of the order of 10^{-10} s, in agreement with available experimental data.

Delivered by Ingenta to: Boulder Labs Library IP: 132.163.130.249 Mon, 21 Aug 2008 19:50:43

When the size of a particle composed by magnetic atoms is small enough, the energy necessary to divide itself into magnetic domains is higher than the energy needed to remain as a single magnetic domain, or monodomain.[46] The magnetic properties of an assembly of monodomain particles is studied within the framework the so-called superparamagnetic theory, name coined by Bean and Livingston[47] in analogy to paramagnetic systems. The first assumption of the superparamagnetic theory is to consider that all the magnetic moments within the particle rotate coherently, i.e., the net magnetic moment can be represented by an single classical vector, with magnitude $\mu = \mu_{at}N$, where μ_{at} is the atomic magnetic moment and N is the number of magnetic atoms that compose such particle. The simplest assumption is to consider an effective uniaxial anisotropy K, which leads to an energy barrier to the magnetization vector which is proportional to KV, where V is the volume of the nanoparticle. It is important to remark, however, that in ultrafine particle systems surface effects can be very important. In such case the magnetic relaxation does not proceed by coherent rotation of the spins within the particle. The influence of the surface will be commented in detail in Section 5.

For a single domain particle with uniaxial anisotropy the magnetic energy can be considered as

$$E_B = KVsen^2\theta - \mu H\cos(\alpha - \theta) \quad (1)$$

where, as illustrated in Figure 1, $\theta(\alpha)$ is the angle between the magnetic moment of the particle (applied field) and the easy axis, KV is the energy barrier that separates both equilibrium states for zero applied field, i.e., $\theta = 0$ and π, and H is the applied field. In absence of external perturbation, the particle magnetic moment can stay in any of the two equilibrium states.

The relaxation of magnetization of these particles can be described by an Arrhenius-type law:

$$M(t) = M_0\exp(-t/\tau) \quad (2)$$

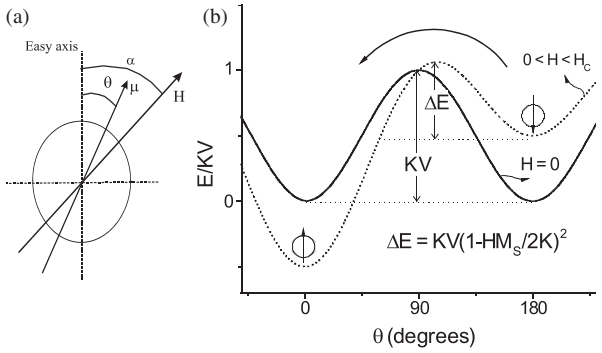

Fig. 1. (a) Definition of the axis system for a fine particle and (b) the angular dependence of the energy barrier for zero external field (continuous line) and for a field value lower than the coercive field (dashed line).

where M_0 is the initial magnetization and τ is the characteristic relaxation time. Such relaxation time is a function of the energy barrier and the temperature:

$$\tau = \tau_0\exp(E_B/k_BT) = \tau_0\exp(KV/k_BT) \quad (3)$$

where k_B is the Boltzmann constant, and τ_0 is inversely proportional to the jump attempt frequency of the particle magnetic moment between the opposite directions of the magnetization easy-axis. The τ_0 values can be experimentally determined and theoretically calculated;[45, 46, 48] ranging[46] between 10^{-9}–10^{-10} s. When a magnetic field is applied, the total energy barrier is given by Eq. (1), the Arrhenius law has an energy barrier lower than KV, as shown in Figure 1.

In granular systems the observed magnetic behaviour strongly depends on the value of the characteristic measuring time τ_m (the time window) of the employed experimental technique with respect to the intrinsic system relaxation time τ, associated to the energy barrier. This time window varies from large values, as in magnetization measurements (typically 100 s) to very small ones, like in Mössbauer spectroscopy (10^{-8} s). If $\tau_m \gg \tau$ the relaxation is faster than the magnetization orientation observed in this time window, allowing the system to reach thermodinamical equilibrium. The nanoparticles are considered to be in the superparamagnetic regime. On the other hand, if $\tau \gg \tau_m$, the system relaxation proceeds very slowly, and one can observe quasistatic properties as in ordered magnetic systems. Such nanoparticles are in the so-called blocked regime. The temperature that divides both regimes is called blocking temperature T_B, and depends on the characteristic measuring time τ_m (defined by $\tau_m = \tau$). T_B is associated to the energy barrier, and for this reason it increases when the particle size increases.

Let us define a critical volume V_{crit} at a certain constant temperature T_0, which requires $\tau_m = \tau$ in Eq. (3):

$$\ln\tau = \ln\tau_0 + \frac{KV_{crit}}{k_BT_0} = \begin{cases} \ln 10^2 \\ \cdots \\ \ln 10^{-8} \end{cases} \quad (4)$$

Therefore, for $\tau_m = 100$ s (a typical measurement time for conventional magnetometry). One has

$$V_{crit} \approx \frac{25\,k_BT}{K} \quad (5)$$

for a given measuring time it is possible to define the blocking temperature T_B, i.e., for a certain fixed volume $V = V_0$ one also sets $\tau_m = \tau$:

$$\ln\tau = \ln\tau_0 + \frac{KV_0}{k_BT_B} = \begin{cases} \ln 10^2 \\ \cdots \\ \ln 10^{-8} \end{cases} \quad (6)$$

Delivered by Ingenta to:
Bucknell Library
IP: 192.163.[illegible]
Mon, 11 Aug 2008 [illegible]
AMERICAN SCIENTIFIC PUBLISHERS

For $\tau_m = 100$ s one obtains the well-known result:

$$T_B \approx \frac{KV_0}{25k_B} \tag{7}$$

The critical volume for superparamagnetism is directly proportional to the temperature, i.e., the higher the temperature, the higher the critical size of the particles; all particles which are smaller than the critical size are in the superparamagnetic regime, i.e., if the system has a grain size distribution, when temperature is increased, more particles fall into the superparamagnetic regime. From Eq. (6) one sees that the blocking temperature is directly proportional to the volume of the particles and its anisotropy constant. In other words, the bigger particles become superparamagnetic at higher temperatures.

It is possible to perform measurements of the blocking temperatures for diferent time windows, by means of Mössbauer spectroscopy, AC susceptibility, and SQUID magnetometry.[49] When such measurements are performed on nanoparticles dispersed on a polymer, in such a way that the interaction among particles becomes negligible, it is possible to corroborate that in very diluted systems the behavior predicted by Eq. (2) is indeed in good agreement with experimental results.

Although apparently simple, the complexity of the problem makes that exact solutions only exist for limiting cases, such as $T = 0$ K, for fully-blocked particles (known as Stoner-Wohlfart model[50]), or for $T \gg T_B$, for a fully superparamagnetic system. The problem becomes even more complicated if one considers magnetic interactions among particles, as the ones evidenced in several real systems using different experimental techniques.[10, 11, 16, 51, 52] Only in the last years, with better computational systems and recent developments in statistical physics, it was possible to make realistic simulations in many-body systems by means of Monte-Carlo techniques.[53–59] There are many simulation models that use different approaches to the problem, and the literature is full of inconclusive results, or even contradictory ones. For example, a still open problem is the role of interactions on the blocking temperature. The majority of simulation results agree that magnetostatic interactions lead to an increase in T_B, in agreement with experimental results,[55, 57] but some results are contradictory.[11]

In order to verify if a system behaves as an ideal superparamagnet, one should initially analyze three aspects:
(i) if the reduced magnetization (M/M_S), plotted as a function of $M_S(H/T)$, results in an universal curve, known as "classical scaling law of superparamagnetism" (see Section 3.1 below),
(ii) if the magnetization isotherms are anhysteretic (see also Section 3.1), and
(iii) if the fitted size distribution is (almost) temperature independent (see Section 3.2).

3. NANOPARTICLE ENSEMBLES

3.1. Langevin Equation

Let us consider an ensemble of magnetic monodomain particles, each with a magnetic moment μ and negligible anisotropy. Despite the fact that the magnetism is basically a quantum effect, one can treat the magnetic moment μ as a classical vector, because every atom's magnetic moment within each particle is considered to be ferromagnetically coupled, and rotating coherently (in unison). Therefore, the statistical treatment of this system can follow the same classical formulation of the paramagnetism, considering bigger magnetic moments (typically of thousands of Bohr magnetons). Let us consider that the system is at a temperature T, under a magnetic field H, and that the thermal equilibrium was already reached. At this temperature all particles are in the superparamagnetic state ($KV \ll k_B T$) and we can consider only the second term of Eq. (1). Therefore, one has now a Boltzmann distribution of the moments μ relative to the field H. Each magnetic moment has a certain potential energy E_B, given by

Delivered by Ingenta to:
Boulder Labs Library
IP : 132.163.130.242
Mon, 15 Aug 2008 19:50:43

$$E_B = -\mu \cdot H = -\mu H \cos\theta \tag{8}$$

The number of moments between θ and $\theta + d\theta$ to the field H is easily found. In the absence of a field the number of vectors passing through unit area of the sphere surface is the same at any point on the sphere surface. Therefore dn is proportional to the area $dA = 2\pi sin\theta d\theta$ (for a sphere of unit radius) multiplied by the Boltzmann factor

$$\begin{aligned} dn &= KdA \exp[-E_p/k_B T] \\ &= 2\pi C \exp[(\mu H \cos\theta)/k_B T] \sin\theta d\theta \end{aligned} \tag{9}$$

where C is a proportionality factor, determined by the condition $\int_0^n dn = n$ calling $a = \mu H/k_B T$, one obtains:

$$2\pi C \int_0^\pi \exp(a\cos\theta)\sin\theta d\theta = n \tag{10}$$

By multiplying the number of the magnetic moments dn and the contribution $\mu\cos\theta$ of each moment, and integrating over the total number of magnetic moments, one obtains the total magnetization M:

$$M = \int_0^n \mu\cos\theta dn \tag{11}$$

$$\begin{aligned} M &= 2\pi C\mu \int_0^\pi \exp(a\cos\theta)\sin\theta\cos\theta d\theta \\ &= \frac{n\mu \int_0^\pi \exp(a\cos\theta)\sin\theta\cos\theta d\theta}{\int_0^\pi \exp(a\cos\theta)\sin\theta d\theta} \end{aligned} \tag{12}$$

$$M = n\mu(\cot h\, a - 1/a) \tag{13}$$

where $n\mu$ is the maximum magnetization value that the system can reach, which corresponds to the perfect aligning of the all magnetic moments to the external field.

This magnetization corresponds to the saturation magnetization M_S:

$$\frac{M}{M_S} = \cot h\left(\frac{\mu H}{k_B T}\right) - \frac{k_B T}{\mu H} = L\left(\frac{\mu H}{k_B T}\right) \quad (14)$$

where L is the famous Langevin function. From Eq. (14) one sees that it is very easy to check if a system is superparamagnetic or not. One just has to make measurements of magnetization versus magnetic field at some temperatures. Plotting all the measurements in a graph of M/M_S versus H/T one expects all curves to converge to a single universal one (Langevin's curve), if the measurement temperature is above the irreversibility temperature. In real systems, however, there are several reasons for not obtaining a good fit of an experimental curve, such as the existence of a distribution of grain sizes, a random anisotropy axis distribution, surface anisotropy, or interparticle magnetic interactions.

These factors affect the expected magnetic response of the system if the thermal energy is not high enough to "erase" its effects. In some cases, even having an almost ideal particle system (noninteracting, narrow size distribution), when thermal energy is much bigger than the total anisotropy of the particle, the proposed scaling law does not work properly. In these cases the inversion of the magnetization does not involve coherent rotation of the spins of the particle.[60] At very high temperatures the surface of the particle can "disconnect" from its core, relaxing in a different way. This is usually manifested as a bimodal behavior in the curves of magnetization versus applied magnetic field, in which it is observed an expected Langeving-like behavior plus a linear component of the magnetization corresponding to the surface. It is possible, in many cases, to subtract the linear component. Nevertheless, when temperature is increased, the particle's core begins "to disarm itself" losing spins that behave as those of the surface. For this reason it is necessary, to recover the scaling law, to plot M/M_S versus HM_S/T.

In the case of systems with interparticle interactions, an apparently good fit of the magnetization curve to the Langevin equation often leads to inconsistent results.[61–63]

3.2. Initial Magnetic Susceptibility

The initial susceptibility of a monodomain particle with volume V, uniaxial anisotropy K and saturation magnetization M_S is:

(i) $T > T_B$: The particle is superparamagnetic and its magnetization is given by the Langevin function. For small values of a, i.e., low magnetic fields or high temperatures, the Langevin function can be expanded as a power series $L(a) = a/3 - a^3/45 + 2a^5/945 - \cdots$, and for $a \to 0$ the Langevin function can be approximated by a straigh line with slope $a/3$. Thus, the particle magnetization is given by

$$M(H,T) = \frac{N\mu^2 H}{3k_B T} \quad (15)$$

and the initial susceptibility for the superparamagnetic particle $\chi_{sp} = M/H$ results $\chi_{sp} = N\mu^2/3k_B T$, being $\mu = M_S V$ the particles magnetic moment, and $N = 1/V$ the density of particles per unit volume. Therefore

$$\chi_{sp} = \frac{M_S^2 V}{3k_B T} \quad (16)$$

which is the well-known Curie law.

(ii) $T < T_B$: The particle is blocked and its magnetization orientates itself in order to decrease the free energy. It is interesting to observe that this process is strongly affected by the magnetic history of the ensemble. In case of that the particles magnetic moment is randomly oriented, the initial magnetization can be calculated by minimizing the Eq. (1). By doing so one obtains the particles initial susceptibility given by:

$$\chi_{bl} = (2/3)\frac{M_S}{H_a} \quad (17)$$

where H_a is the so-called anisotropy field, $H_a = 2K/M_S$. The initial susceptibility is therefore

$$\chi_{bl} = \frac{M_S^2}{3K} \quad (18)$$

3.3. Grain Size Distribution and Measurement Techniques

Real particle systems have particle size distribution. For instance, a transmission electron microscopy (TEM) image of a sample composed of almost periodically arranged Co nanoparticles immersed on a SiO_2 matrix is shown in Figure 2. Details of sample production can be seen in Ref. [64]. The particle size distribution (see Fig. 2) was obtained measuring the particle sizes in images of several different parts of this sample, and is well fitted by a Gaussian distribution, giving an average diameter of 3 nm.

For each particle size distribution there is its corresponding particle moment distribution. For a given magnetic

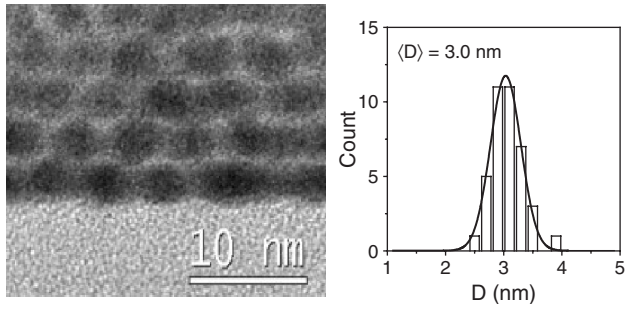

Fig. 2. Cross section TEM image of the granular multilayer (left). The average diameter of the particles is 3 nm, as shown in the size distribution (right). Reprinted with permission from [119], J. C. Denardin et al., *Physica B* 384, 290 (**2006**). © 2006, Elsevier.

Delivered by Ingenta to:
Boulder Labs Library
IP: 132.163.130.249
Mon, 17 Aug 2009 19:56:49

REVIEW

moment distribution, $f(\mu)$, the macroscopic magnetization is given by:[9, 65]

$$M(H,T) = \int_0^\infty \mu L\left(\frac{\mu H}{k_B T}\right) f(\mu) d\mu \qquad (19)$$

In order to apply Eq. (19) to experimental data one has to consider an appropriate distribution function for the magnetic moments. Electron microscopy images indicate that the size distribution in granular systems often follows a log-normal distribution function of the type:[9, 41, 66]

$$f(\mu) = \frac{N}{\sqrt{2\pi}} \exp\left[-\frac{\ln^2(\mu/\mu_0)}{2\sigma^2}\right] \qquad (20)$$

Based on the given definition, the mean magnetic moment is given by $\langle\mu\rangle = \mu_0 \exp(\sigma^2/2)$. In this way, the parameters μ_0 and σ can be obtained through appropriate fits to the experimental magnetization curve. Moreover, if one considers that the particles have spherical shape, it is possible to obtain size distribution, particle density and average distance among them.[66]

The basic characterization technique is the measurement of the magnetization as a function of temperature or applied external field (hysteresis loop). The first procedure is usually done following zero-field-cooling (ZFC) and field-cooling (FC) magnetization measurement protocols, which indicate the mean blocking temperature and also provide information on the particle size distribution.[13, 67] Figure 3 shows a typical curve from a ZFC-FC measurement of a sample of Co-Ni-B particles dispersed in a polymer,[66] where one can distinguish three characteristic temperatures: the blocking temperature (T_B), as the temperature of the maximum of the ZFC curve; the irreversibility temperature, which is the temperature where the ZFC magnetization curve departs from the FC one; and the temperature of the maximum of $d(M_{FC} - M_{ZFC})/dT$ versus T. The former curve gives one information about the energy barrier distribution. When the anisotropy is proportional to the volume, as in the present case, it is proportional to the size distribution profile.[2]

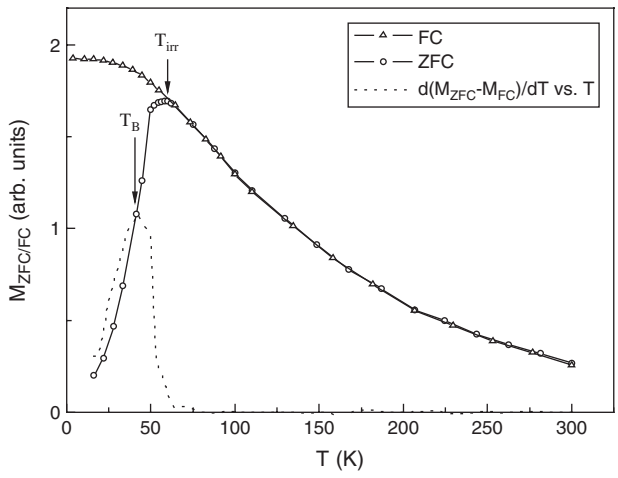

Fig. 3. Typical ZFC-FC measurement of a sample of Co-Ni-B particles dispersed in a polymer. The irreversibility temperature (T_{irr}) and the mean blocking temperature (T_B) are indicated.

It is possible to directly follow the time relaxation of the magnetization in order to extract relevant information on the energy barriers (see more details in Section 3.8). Another useful experimental technique is the AC susceptibility, where different frequencies of the excitation field are employed to investigate the relaxation process. When the frequency changes, the number of nanoparticles that follow the oscilations of the magnetic field vary, thus modifying the magnetic response.[2] One technique that provides a new frequency window is the transversal dynamic susceptibility,[68] which is the variation of the magnetization due to a small alternating magnetic field, applied perpendicular to the DC field. The advantage of such technique is the possibility to perform measurements in the radio frequency (RF) range, and the capability to disclose the singularities of the magnetization curves in the anisotropy field H_a.[68] In fact, magnetization dynamics is one of the key issues of magnetic materials for novel data storage devices. The magnetization dynamics of two-dimensional (2D) devices employed in magnetic random access memories (MRAMs) is determined by the 2D magnetization switching properties, because the MRAM cells require a magnetic field that is applied in the plane of the device. In addition, the study of two-dimensional magnetic switching behaviour enables one to determine the critical curve,[69] which provides information about micromagnetic and structural properties of magnetic systems.[70]

Another technique widely used in the study of superparamagnetic systems is the Mössbauer spectroscopy, which uses the resonance of certain isotopes (the most important ^{57}Fe) to measure the hyperfine magnetic field. Due to the relationship between magnetic moment and hyperfine magnetic field one can get another view of the nanostructured system.[71, 72] An alternative use of the Mössbauer spectroscopy is the thermal scanning, which provides information regarding Curie temperature[73, 74] and fractions of magnetic phases.[75]

3.4. Typical Measurements for Magnetic Characterization of Granular Systems: ZFC and FC Magnetization Curves

One possible way to measure the initial susceptibility of a sample is by demagnetizating it at a temperature higher than the blocking one (where all particle moments are randomly oriented), and afterwards cooling it without applied field down to a temperature much lower than T_B, to finally apply a small field H_m to measure magnetization during the subsequent temperature rise. The obtained curve is called zero-field-cooled (ZFC) magnetization. One can obtain a complementary curve by doing the same process,

but cooling the sample with a small applied field (called field-cooled magnetization, FC). Both curves provide valuable information on the nanostructure.

The susceptibility of an ensemble of particles, with volume distribution $p_v(V)$ and uniaxial anisotropy K, was calculated by Chantrell et al.[76] The fraction of particles with volumes between V and $V+dV$ is given by $p_v(V)dV$, that can be obtained, for example, by a histogram built from transmission electron microscopy (TEM) images, or Small Angle X-ray Scattering (SAXS) spectra.[74, 77] Once the size distribution is known, it is easy to obtain the mean particle volume:

$$\langle V\rangle = \int_0^\infty V p_v(V)\,dV \tag{21}$$

As defined above, for each temperature T there is a critical volume $V_c(T) = 25k_BT/K$, which marks the limit between the superparamagnetic particles ($V < V_c(T)$) and the blocked ones ($V > V_c(T)$). Thus, the contribution for the susceptibility of the superparamagnetic particles can be obtained using the initial susceptibility discussed in Section 3.2,

$$\int_0^{V_c} \chi_{SP}(V)p_v(V)\,dV = \int_0^{V_c}\left(\frac{M_s^2 V}{3k_BT}\right)p_v(V)\,dV \tag{22}$$

and the contribution of the blocked fraction is given by

$$\int_{V_c}^\infty \chi_{bl}(V)p_v(V)\,dV = \int_{V_c}^\infty\left(\frac{M_s^2}{3K}\right)p_v(V)\,dV \tag{23}$$

When measuring zero-field-cooled (ZFC) magnetization, one has to cool down the sample below T_B. The susceptibility (M_{ZFC}/H_m), for an applied field much smaller than the anisotropy field ($H_m \ll H_a$), can be written as

$$M_{ZFC}/H_m = \left(\frac{M_s^2 V}{3k_BT}\right)\int_0^{V_c} V p_v(V)dV + \left(\frac{M_s^2}{3K}\right)\int_{V_c}^\infty p_v(V)dV \tag{24}$$

Equation (24) can be simplified by using reduced variables $t_B = T_B/\langle T_B\rangle = V/\langle V\rangle$ and $t = T/\langle T_B\rangle$ (the symbols between brackets indicating mean values).

$$(M_{ZFC}/M_s)(3K\langle V\rangle/M_sH_m) = (K\langle V\rangle/k_BT)\int_0^{T/\langle T_b\rangle} t_b\cdot p_{t_b}(t_b)\,dt_b + \int_{T/\langle T_b\rangle}^\infty p_{t_b}(t_b)\,dt_b$$

$$(M_{ZFC}/M_s)(3K\langle V\rangle/M_sH_m) = \frac{25}{t}\int_0^t t_b\cdot p_{t_b}(t_b)\,dt_b + \int_t^\infty p_{t_b}(t_b)\,dt_b \tag{25}$$

The FC magnetization M_{FC} is very similar to the expression for M_{ZFC}, the contribution coming from the superparamagnetic particles being the same, and the contribution from the blocked ones does not depend on T. The only difference is that the contribution from the blocked particles to the magnetization is not that of a random oriented magnetic moment ensemble, as in the case of ZFC. One can assume it to be the magnetization value reached at the blocking temperature T_B, i.e., $\chi_{sp}(T_B)H_m$:

$$(M_{FC}/M_s)(3K\langle V\rangle/M_sH_m) = \int_0^t (25/t)t_b\cdot p_{tb}(t_b)\,dt_b + (H_c/H_m)\int_t^\infty (25/t_b)t_b\cdot p_{tb}(t_b)\,dt_b$$

$$(M_{FC}/M_s)(3K\langle V\rangle/M_sH_m) = (25/t)\int_0^t t_b\cdot p_{tb}(t_b)\,dt_b + 25(H_c/H_m)\int_t^\infty p_{tb}(t_b)\,dt_b \tag{26}$$

If one considers $H_c \approx H_m$:

$$(M_{FC}/M_s)(3K\langle V\rangle/M_sH_c) = (25/t)\int_0^t t_b\cdot p_{tb}(t_b)\,dt_b + 25\int_t^\infty p_{tb}(t_b)\,dt_b \tag{27}$$

It is easy to see that the difference between the FC and ZFC curves is basically that the contribution of the blocked particles is 25 times larger in the FC than in the ZFC curve. As previously discussed, the $f(T_B)$ can be related to the distribution of particle sizes by the linear expression $25k_BT_B = KV$, where V is the particle volume. Therefore one can obtain K by fitting the ZFC curves using a

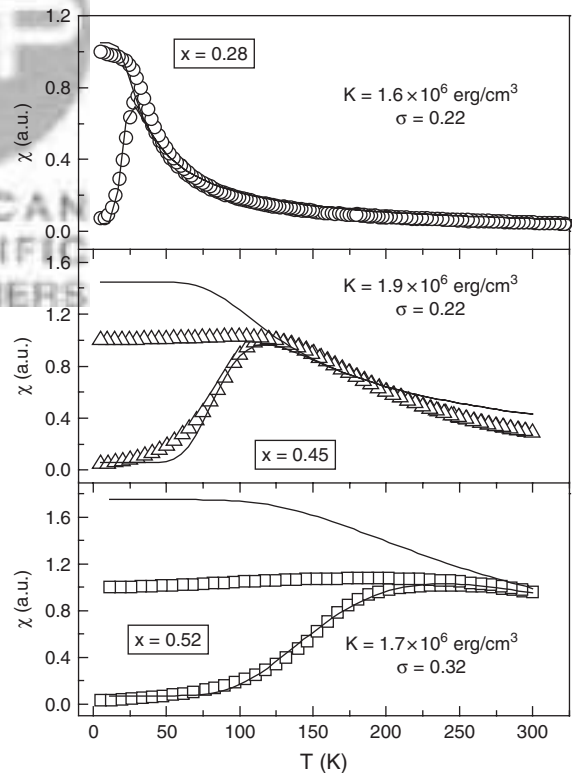

Fig. 4. Zero field cooled and field cooled curves measured for samples of $Co_x(SiO_2)_{1-x}$, with $x = 0.28$, 0.45, and 0.52, respectively. The lines are fits using Eqs. (25) and (27) using a particle size distribution obtained through SAXS experiments.

Delivered by Ingenta to: Boulder Labs Library IP : 132.163.150.249 Mon, 11 Aug 2008 19:50:43
AMERICAN SCIENTIFIC PUBLISHERS

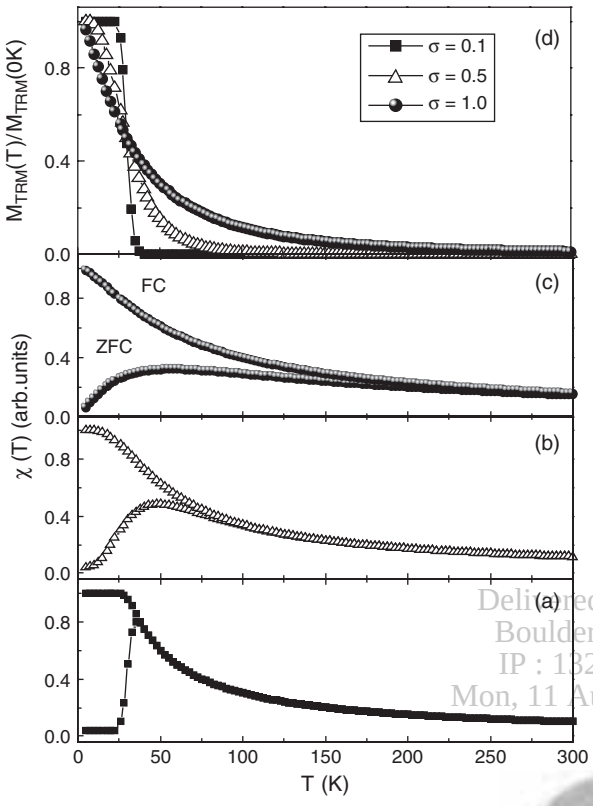

Fig. 5. ZFC, FC, and TRM curves calculated with Eqs. (25), (27) and (28), respectively, considering a blocking temperature of $T_B = 30$ K and different particle size distributions ($\sigma = 0.1$, 0.5, and 1).

proper distribution obtained by SAXS or TEM measurements, for example. Figure 5 shows the result obtained by fitting the above expressions to the ZFC and FC curves measured with an applied field of 20 Oe in $Co_x(SiO_2)_{1-x}$ samples with three different Co concentrations. As can seen in Figure 4, the superparamagnetic model is a good approach to describe the ZFC and FC curves of the more diluted samples. Moreover, although the effective magnetic anisotropy values obtained for samples are significantly larger than those expected for bulk samples, the fitting procedure does not lead to large anisotropy values for the more concentrated sample (see values in Fig. 4). This behaviour clearly disagrees with the anisotropy size dependence of the barrier discussed in Section 2, since the mean particle diameter is larger for more concentrated samples. A model that considers the effect of magnetic interactions in T_B will be discussed in Section 4.2.

3.5. TRM Curves

Another type of interesting magnetic characterization is the so-called thermoremanent magnetization (TRM), where the saturation field is applied at temperature higher than T_B. Then the sample is cooled down to a temperature lower than T_B, where the field is switched off, and after around 100 s the sample magnetization is measured. A remanence curve is obtained by raising the temperature, where for each value of T the very same procedure is performed. Because $H_m = 0$, there is no contribution of any susceptibility, so that one can assume that the magnetization of the blocked particles is simply the remanent magnetization M_r:

$$(\mathrm{TRM}/M_s) = 0 + \gamma \int_t^\infty p_{tb}(t_b)\, dt_b \tag{28}$$

where the factor γ depends on the mean orientation of the randomly-distributed magnetic moments, and is 0.5 for an hemisphere (uniaxial anisotropy). If the anisotropy were cubic, $\gamma = 0.886$. Obviously, this approximation is valid only if the particles are independent (no magnetic interaction among them).

3.6. Log-Normal Size Distribution

As previously mentioned, volume distributions in granular systems often follow log-normal-type functions:

$$p_{tb}(t_b) = \frac{1}{\sqrt{2\pi\sigma^2}} \frac{1}{t_b} \exp\left[-\frac{\ln^2(t_b)}{2\sigma^2}\right] \tag{29}$$

where σ is the variance around $\ln(t_b)$. In log space, by using $\varepsilon = ln(t)$ one has

$$p_{\varepsilon^b}(\varepsilon_b) = [dt_b/d\varepsilon_b] \cdot p_{tb}[t_b] = [\exp(\varepsilon_b)] \cdot p_{tb}[\exp(\varepsilon_b)] \tag{30}$$

which results in

$$p_{\varepsilon^b}(\varepsilon_b) = \frac{1}{\sqrt{2\pi\sigma^2}} \frac{\exp(\varepsilon_b)}{\exp(\varepsilon_b)} e^{-\frac{\varepsilon_b^2}{2\sigma^2}} = \frac{1}{\sqrt{2\pi\sigma^2}} e^{-\frac{\varepsilon_b^2}{2\sigma^2}} \tag{31}$$

which is the normal distribution (gaussian), of variance σ.

The contribution from the blocked particles for ZFC, FC, and TRM measurements, with the proper prefactors, can be written as:

$$\int_t^\infty p_{tb}(t_b)\, dt_b = \int_\varepsilon^\infty p_{\varepsilon^b}(\varepsilon_b)\, d\varepsilon_b = 1 - \mathrm{ERF}[\varepsilon, \sigma] \tag{32}$$

where the error function is

$$\mathrm{ERF}[\varepsilon, \sigma] = \frac{1}{\sqrt{2\pi\sigma^2}} \int_{-\infty}^{\varepsilon} e^{-\frac{\varepsilon_b^2}{2\sigma^2}}\, d\varepsilon \tag{33}$$

Some algebra is necessary to get such contribution

$$t_b \cdot p_{tb}(t_b) = \frac{1}{\sqrt{2\pi\sigma^2}} \frac{t_b}{t_b} e^{-\frac{\ln^2(t_b)}{2\sigma^2}} = \frac{1}{\sqrt{2\pi\sigma^2}} e^{-\frac{\ln^2(t_b)}{2\sigma^2}} \tag{34}$$

then, by using $t_b = \exp(\varepsilon_b)$ and $p_{tb}(t_b)dt_b = p_{\varepsilon^b}(\varepsilon_b)d\varepsilon_b$:

$$\begin{aligned} t_b \cdot p_{tb}(t_b)dt_b &= 1/(2\pi\sigma^2)^{1/2} \exp(\varepsilon_b) p_{\varepsilon^b}(\varepsilon_b) d\varepsilon_b \\ &= 1/(2\pi\sigma^2)^{1/2} \exp(\varepsilon_b) \cdot \exp[-\varepsilon^2/2\sigma^2] d\varepsilon_b \end{aligned} \tag{35}$$

Delivered by Ingenta to:
Boulder Labs Library
IP : 132.163.130.249
Mon, 11 Aug 2008 19:50:43

that can be rewritten as

$$\begin{aligned} t_b \cdot p_{tb}(t_b)dt_b &= 1/(2\pi\sigma^2)^{1/2}\exp[-(1/2\sigma^2) \\ &\quad \cdot(\varepsilon_b^2 - 2\sigma^2\varepsilon_b)]d\varepsilon_b \\ &= 1/(2\pi\sigma^2)^{1/2}\exp[-(1/2\sigma^2) \\ &\quad \cdot(\varepsilon_b^2 - 2\sigma^2\varepsilon_b + \sigma^4) + \sigma^2/2]d\varepsilon_b \\ &= 1/(2\pi\sigma^2)^{1/2}\exp[\sigma^2/2]\exp[-(1/2\sigma^2) \\ &\quad \cdot(\varepsilon_b - \sigma^2)^2]d\varepsilon_b \end{aligned} \tag{36}$$

In this way one can write

$$\begin{aligned} (1/t)\int_0^t &= t_b \cdot p_{tb}(t_b)\,dt_b = \exp(-\varepsilon) \\ &= \int_{-\infty}^{\varepsilon} \exp[\sigma^2/2]\exp[-(1/2\sigma^2)\cdot(\varepsilon_b - \sigma^2)^2]d\varepsilon_b \\ &= \exp[\sigma^2/2]\cdot\exp(\varepsilon)\cdot \mathrm{ERF}[(\varepsilon - \sigma^2), \sigma] \end{aligned} \tag{37}$$

Delivered by Ingenta to:
Boulder Labs Library
IP : 132.163.130.240
Mon, 11 Aug 2008 19:50:43

to finally obtain

$$\begin{aligned} (1/t) &= \int_0^t t_b \cdot p_{tb}(t_b)\,dt_b = \exp(-\varepsilon) \\ &= \int_{-\infty}^{\varepsilon} \exp(\varepsilon_b)\cdot p_{\varepsilon^b}(\varepsilon_b)\,d\varepsilon_b \\ &= \exp[\sigma^2/2]\cdot\exp(-\varepsilon)\cdot \mathrm{ERF}[(\varepsilon - \sigma^2), \sigma] \end{aligned} \tag{38}$$

Figure 5 shows ZFC, FC, and TRM curves calculated with the above equations. Curves are plotted as functions of the reduced temperature, and were calculated for $\sigma =$ 0.1, 0.5, and 1, respectively, considering the same average magnetic moment μ. It is clear that when the size distribution width (σ) is increased, ZFC and FC curves separate from each other at higher temperatures. This well known effect, caused by the wider variation in particle sizes, can be explained in the following way: in the ZFC curve the system departs from a fully disordered state, and a fraction of particles will be unblocked at higher temperatures, above the temperature of the maximum in ZFC curve. These particles, that do not contribute to the raise of the magnetization in the ZFC curve (because they are randomly oriented, averaging its contribution to zero) can contribute to the FC curve, because they are unblocked and will be cooled with applied field H_m. If the particle size does not vary so much in the sample, as the case of $\sigma = 0.1$, practically all the particles will be unblocked in a small temperature interval, and they contribute in the same way for the magnetization in ZFC and FC curves. The TRM curves are shown in Figure 5(d) for different values of σ, where one can observe that the temperature where the remanence falls to zero occurs at lower temperatures when σ increases. One can also observe that all TRM curves intercept at the inflection point, i.e., $T = \langle T_B \rangle =$ 30 K in the presented simulation.

When dealing with size distributions one needs to take care in the conversion from diameter to volume (or blocking temperature), mainly when the distribution is not symmetric, as in the case of log-normal, and the transformation is not linear. There are three quantities that can be used for measuring a position in a distribution:
(i) The typical value, or mode, which is the position of the density probability maximum;
(ii) The median, which is the position that splits the population by the half (50% above and 50% below).
(iii) The mean value, which is the distribution "gravity center."

For a symmetrical distribution all three positions have the same value, but for assymetrical ones, they are different. Let's see how is done a transformation into a log-normal distribution, given by:

$$f(D) = \frac{1}{\sqrt{2\pi\sigma_D^2}}\frac{1}{D}\exp\left(-\frac{\ln^2\left(\frac{D}{\langle D\rangle}\right)}{2\sigma_D^2}\right) \tag{39}$$

From this distribution one can easily calculate the mode: $\langle D\rangle \exp(-\sigma_D^2)$; the median: $\langle D\rangle$; and the mean value: $\langle D\rangle \exp(\sigma_D^2/2)$. Also, it is interesting to calculate a volume distribution from the particles diameter distribution. Considering that $f(V)dV = f(D)dD$ and $V = D^3\pi/6$, one has $dV/dD = \pi D^2/2$ and thus $f(V) = (2/\pi D^2)f(D)$. Therefore it is straightforward to show that the volume dispersion is just three times the diameter dispersion, $\sigma_V = 3\sigma_D$.

3.7. Coercive Field

The magnetization curve for a system of magnetic monodomains in the blocked state ($T = 0$) was calculated by Stoner and Wohlfarth,[50] and the values of the coercivity can turn out to be rather large. Some assumptions are made to perform the calculation:
(i) monodisperse nanoparticle system with uniaxial anisotropy;
(ii) random distribution of easy axis; and
(iii) coherent reversal of the magnetic moments of the particles.

The magnetization curve thus calculated results in a remanence equal to the half of M_S, and a coercive field (see Refs. [46 and 50] for details),

$$H_C = 0.48\frac{2K}{M_s} \tag{40}$$

The effect of temperature on the reversal of the particles was presented by Bean and Livingston for a single particle of volume V. They considered thermally activated magnetization reversal at a certain temperature T. In this way, the maximum anisotropy barrier for thermally activated magnetization switching has the value $25k_BT$. Therefore, for $T < T_B$ the particle has irreversible magnetization reversal, because in order to occur a magnetization reversal is

necessary to apply an external field to reduce the energy barrier down to $25k_BT$. The effect of the field in the energy barrier is shown in Figure 1. The field value that lowers the barrier energy to $25k_BT$ is the coercive field, i.e.,

$$KV\left(1-\frac{H_{C1}M_S}{2K}\right)^2 = 25k_BT \tag{41}$$

By considering Eq. (7) and after simple algebra, one obtains the expression for the coercive field of a single particle of volume V:

$$H_{C1} = \frac{2K}{M_S}\left[1-\left(\frac{25k_BT}{KV}\right)^{1/2}\right] = \frac{2K}{M_S}\left[1-\left(\frac{T}{T_B}\right)^{1/2}\right] \tag{42}$$

However, this expression of the coercive field was obtained by considerin just one particle with volume V. The coercive field of an ensemble of such particles can be obtained by considering the Stoner-Wohlfarth model (H_C for $T=0$ should be $0.48(2K/M_S)$) in the equation above. Thus, the coercive field of a system of nanoparticles would be given by

$$H_C = 0.48\frac{2K}{M_S}\left[1-\left(\frac{T}{T_B}\right)^{1/2}\right] \tag{43}$$

Although this equation does not consider a size distribution, it is widely used in the study of magnetic properties of such systems. The incorporation of the particle size distribution on the temperature dependence of coercive field, $H_C(T)$ is not an easy task, because net H_C is not a simple superposition of individual particle coercivities.

The $H_C(T)$ behavior considering particle size distribution was recently described by a rather simple phenomenological approach.[78] In this model, both blocking temperature distribution and unblocked particles contributions were considered. The coercive field of the blocked particles is obtained by means of

$$H_{CB} = 0.48\frac{2K}{M_S}\left[1-\left(\frac{T}{\langle T_B\rangle_T}\right)^{1/2}\right] \tag{44}$$

where K is the anisotropy constant, M_S the saturation magnetization, and $\langle T_B\rangle_T$ is the average blocking temperature, which takes into account only the volume fraction of blocked particles at temperature T. Notice that $\langle T_B\rangle_T$ is different from the average blocking temperature $\langle T_B\rangle$.

As any real system has a distribution of volumes (and consequently a blocking temperature distribution, $f(T_B)$), the total coercive field can be calculated by averaging the magnetization of superparamagnetic and blocked particles,

$$\langle H_C\rangle_T = \frac{M_r(T)}{\chi_S(T)+[M_r/H_{CB}]} \tag{45}$$

where $M_r(T)$ is the remanence for different temperatures and $\chi_S(T)$ the susceptibility of the particles that are superparamagnetic at a certain temperature T. To obtain $H_C(T)$ through Eq. (45), three terms must be evaluated: $M_r(T)$, $\chi_S(T)$, and $H_{CB}(T)$, all determined from experiments. For the last two terms, a good determination of $f(T_B)$ is needed, which can be obtained by the ZFC-FC and thermoremanent magnetization curves as presented in Sections 4.1 and 4.2.

Figure 6 shows the comparison between the experimental $H_C(T)$ of a granular $Cu_{90}Co_{10}$ ribbon and calculated curves obtained by different approaches and $f(T_B)$ obtained from thermoremanent magnetization. The dotted line is the standard and widely used Eq. (43), which indeed works for well isolated and rather narrow size distributions. By considering the effect of the unblocked particles, an excellent agreement is obtained at low temperatures, where most of the particles are still blocked. The solid line describes well the results in the whole temperature range. This curve is obtained by taking into account both $\langle T_B\rangle_T$ and the superparamagnetic effect (Eqs. (44) and (45)), i.e., by considering the temperature dependence of the average blocking temperature and the superparamagnetic susceptibility of the unblocked particles.

Finally, it is worth noting that several studies show important effects of magnetic interactions on the coercive field.[55, 79] Interestingly, Kechrakos and Trohidou suggested, by analising Monte Carlo simulations, that the coercive field should decrease with particle density at the low temperature region ($T \ll T_B$), while at temperatures near T_B the coercive field should increase. Moreover, a shift between the calculated and experimental data was observed on the temperature dependence of the coercive field for low nanoparticle concentrations.[78] Similar behaviour was also observed in a γ-Fe_2O_3 nanoparticle system.[79] The appoximately spherical samples were obtained by means of a colloidal method, resulting in a rather narrow size distribution. The strength of the dipolar interaction among nanoparticles was controlled by diluting

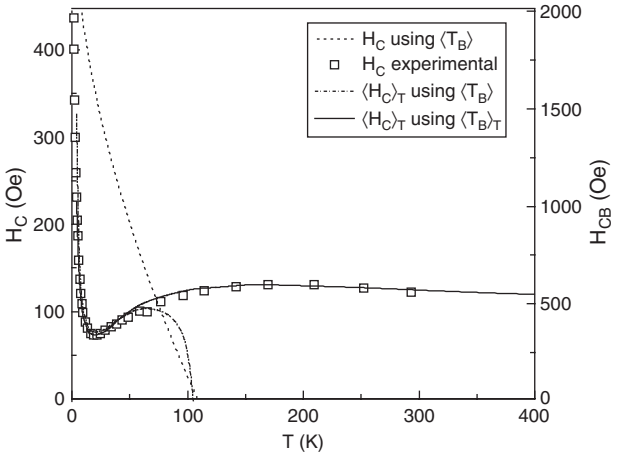

Fig. 6. Experimental and calculated coercive fields versus temperature for a granular $Co_{10}Cu_{90}$ sample. Reprinted with permission from [78], W. C. Nunes et al., *Phys. Rev. B* 70, 014419 (**2004**). © 2004, American Physical Society.

Delivered by Ingenta to:
Stanford Labs Library
IP : 132.163.135.245
Mon, 11 Aug 2008 19:20:43

the same original sample in different amounts of paraffin, allowing the authors to systematically study the effect of dipolar interactions solely, avoiding variations in composition, size distribution or magnetic anisotropy among samples.[79]

The $H_C(T)$ curves calculated using Eqs. (44) and (45), and $f(T_B)$ obtained from ZFC-FC curves ($H = 5$ Oe) are shown in Figure 7 by dashed-lines. The saturation magnetization considered[80] was $M_S = 420$ emu/cm^3 (bulk value), and consequently the only free parameter of the fit was K, that gave the value $K = 2.9 \times 10^5$ erg/cm^3 independently of the dilution of particles. As can be seen in Figure 7, the agreement between theoretical and experimental curves is good only for the more diluted sample. As previously observed in Ref. [81], there is a shift between the theoretical and experimental data for other samples, that increases with particle concentration, thus reinforcing the hypothesis that this observed behaviour is related to interaction among particles.

In order to obtain a better description of the $H_C(T)$ experimental data for the two most concentrated samples, one needs to use $f(T_B)$ obtained from ZFC-FC curves measured under an applied fields higher than 5 Oe. The $H_C(T)$ curves that gave the best agreement with the experimental data are shown by solid lines in Figure 7. The same figure shows the field values used to measure the ZFC and FC curves, which provide the $f(T_B)$.[41]

The physical meaning of the results depicted above was studied in more detail using the ΔM technique which is based on the comparison of the isothermal remanent magnetization (IRM), and the dc demagnetizing remanence (DCD) curves.[82] The IRM curve is obtained by measuring the remanence from the initially demagnetized state and cycling the field between zero and a progressively increasing positive value; the DCD curve is obtained by measuring the remanence with progressively increasing demagnetizing field in a previously saturated sample. It is expected $\Delta M = 0$ for a noninteracting system. However, while in the IRM the initial state of the particles have randomly oriented moments, in DCD the moments are aligned. As the effect of interaction depends on the moment configuration, then the ΔM curve can give relevant information about the strength of such interactions. For example, the obtained results of ΔM for different γ-Fe_2O_3 nanoparticle concentrations are in agreement with the demagnetizing role played by the dipolar interaction,[79] as predicted by Kechrakos and Trohidou by means of Monte Carlo simulations.[34] Thus, the shift towards higher temperatures with increasing concentration can be explained by the demagnetizing role played by the dipolar interaction as observed in ΔM curves since the $H_C(T)$ and ZFC-FC curves have different initial configurations of the magnetic moments.[83, 84]

Delivered by Ingenta to:
Boston Labs Library
IP: 192.163.130.249
Wed, 17 Aug 2008 19:50:43

3.8. Time Relaxation

This type of experiment is useful to study relaxation dynamics of system of nanoparticles at different temperatures. Equation (2) shows that the time dependence of the magnetization of a system of noninteracting, monodisperse, monodomain nanoparticles, with coherent reversal of magnetization, should follow an Arrhenius law. We will consider the case in which a narrow size distribution is present and considering valid all the above mentioned remaining suppositions. Because the magnetization reversal occurs by means of a thermally activated process, it

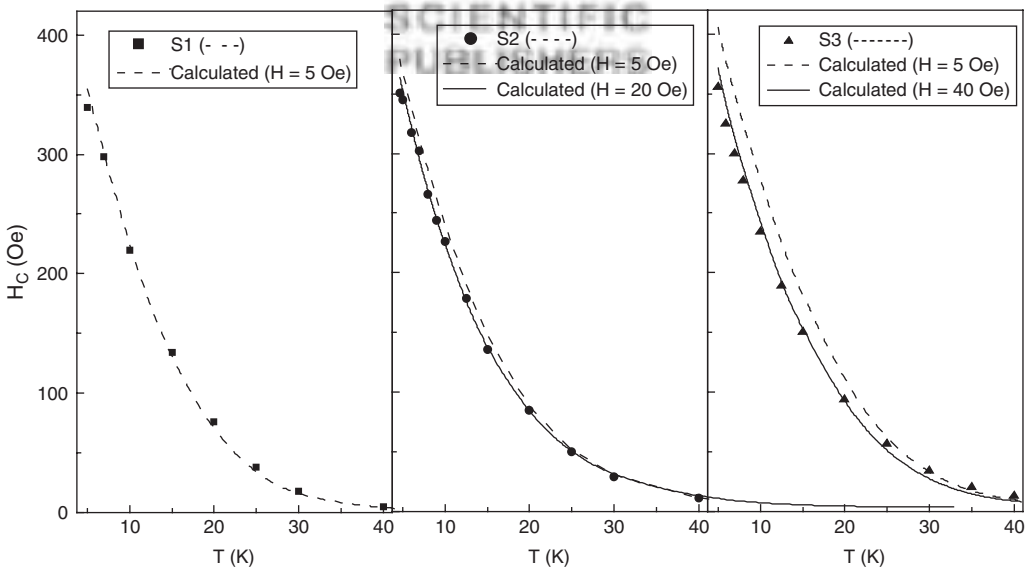

Fig. 7. Symbols: $H_C(T)$ measured for samples of the γ-Fe_2O_3 nanoparticle system. The dashed lines $\langle H_C \rangle_T$ calculated using $f(T_B)$, which were obtained from ZFC-FC curves measured with applied field $H = 5$ Oe. Solid lines: $\langle H_C \rangle_T$ calculated for different samples using convenient values of applied field. Reprinted with permission from [79], W. C. Nunes et al., *J. Appl. Phys.* 99, 08N705 **(2006)**. © 2006, American Institute of Physics.

is possible to find a universal expression for $M(t)$ at different temperatures, leading to important information on the characteristic relaxation time of the nanoscopic system. The measurement can be made in two different ways, both starting from the superparamagnetic state (temperature higher than the irreversibility temperature). The first way consists on cooling the system without applied field (ZFC) until the desired temperature is reached (obviously lower than the irreversibility one). Then, an external field is applied and the magnetization is measured as a function of time. The probability of magnetizing each particle in the direction of the field depends on its characteristic time response, which is, in turn, related to the energy barrier (Eq. (3)). Thus, the total response of the magnetization will also be a function of the size distribution. The second way is to cool the sample with an applied field (FC mode), then removing it to measure the magnetization decay as a function of time. Unlike the previous method, the energy barrier is not modified by the presence of the magnetic field, and therefore one obtains non-perturbed information about the nanoparticles.

Owing to the size distribution, the expression of the relaxation time given in Eq. (3) must be modified in the following way:

$$\tau = \tau_0 \int f(V) \exp(KV/k_B T)\, dV \quad (46)$$

were $f(V)$ is the volume distribution. Nevertheless, if the time window is not very wide, i.e., around few hours, and the size distribution is narrow; the exponential function will be non zero in only a small surrounding, so KV varies between $26k_B T$ and $33k_B T$, approximately.[85] If one performs a time relaxation in the FC mode, after turning off the field, one can write:

$$M(t, T) = C(T) - S(T, t) M_0 \ln(t/\tau_0) \quad (47)$$

where C is a constant that depends on the temperature and the magnetic field at which the FC process was made and S is magnetic viscosity. At $t = \tau_0$ the magnetization of the system is C. This magnetization is directly associated to the magnetization of the system reached after the FC procedure; that is to say, its value depends on the contribution of those particles that are blocked at the temperature in which the measurement is done. Magnetization measured in FC mode in "a well behaved" system presents a monotonous and smooth behavior as a function of temperature, so Eq. (47) leads to a universal law.

One can obtain an expression for magnetic viscosity.[86] This is given by:

$$S = \frac{1}{M_0} \frac{\partial M(t)}{\partial \ln(t)} \approx \frac{(M_0 - M_1)}{M_0} f(k_B T \ln(t/\tau_0)) k_B T \quad (48)$$

where M_0 corresponds to the initial remanent magnetization and M_1 is the magnetization expected when the thermodynamic equilibrium is reached (it could be zero in the abscence of magnetic field). The dependence of f with temperature is practically negligible, thus the magnetic viscosity is proportional to temperature. This has a great importance because it provides an important tool that allows one to get information on the microscopic mechanisms involved in the rotation of the particle magnetic moment, that could depend on the magnetic interactions (among particles) as well as surface effects.[60]

4. INTERACTING SUPERPARAMAGNETIC SYSTEMS

The superparamagnetic model shown in the previous sections is widely used in the analysis of magnetic data, usually neglecting interaction effects among nanoparticles. However, in rather concentrated systems the nanoparticles are close enough for interactions among them become noticeable, affecting the macroscopic magnetic properties. Although substantial progress has been achieved in this research area, one of the major theoretical challenges still to be understood is the role of dipolar interactions among magnetic nanoparticles on the magnetic and magnetotransport properties of such systems. Besides the fundamental scientific interest, the development of manageable theoretical models is the paramount to the advance of the next generation of magnetic recording media, whose magnetic units (bits) are currently achieving nanometric dimensions. In fact, there is a huge number of experimental studies that have evidenced the crucial role of magnetic interactions on the macroscopic physical properties, giving rise to intriguing results such as spin-glass-like behaviour,[87–90] shift of blocking temperature,[11, 91] the existence of a slight hysteresis in fully superparamagnetic systems,[48] the coercivity shift with concentration,[79, 92, 93] the lack of agreement between magnetic and structural data[62, 93, 94] and specific signatures on the magnetization dependence of the giant magnetoresistance.[10] Furthermore, Monte Carlo simulations have confirmed some experimental results,[53, 95] despite the intrinsic requirement of several approximations resulting in a wide variety of numerical data.[55, 96]

In granular nanomagnetic systems there are different types of interactions among nanoparticles: RKKY[a] (present when the matrix is metallic), dipolar, direct exchange (among touching nanoparticles) or even superexchange.[97] It is extremely difficult to test theoretical models in real systems, because the combined effect of interactions, nanoparticle shape, distribution of sizes and anisotropy axes, not to mention surface effects and surface-core interactions.[98, 99] In more concentrated systems, nanoparticles are touching each other, fact that further modifies magnetic and magnetotransport properties.[97, 100, 101]

[a]Long-range, oscilatory interaction among spins mediated by the conduction electrons, the name is due to Ruderman, Kitel, Kasuya, Yoshida, who established the characteristics of this interaction.

Delivered by Ingenta to:
Boulder Labs Library
IP : 132.163.150.245
Mon, 11 Aug 2008 19:50:45

Superferromagnetism is a term that was coined to describe a collective behavior in clusters of nanoparticles, which results in a large effective magnetic nanoparticle.[102] This concept partially explains some observed discrepancies between magnetic and structural data,[41, 102] but is not complete enough to explain all the experimentally observed behaviours. Generally speaking, two main models[103, 104] have been applied in the last years. In the Hansen-Mørup approach, a mean field approximation is used to describe the effect of interactions.[103] The predictions of such model agree with experimental data in the highly concentrated regime, but seem to contradict several experimental results.[105] In the Dormann-Bessais-Fiorani model the effect of interactions is introduced through energy barriers affecting individual particles. This model reproduces correctly the variation of the blocking temperature as a function of the observation time window of the experiment.[67] However, this approach oversimplifies the physical situation, because it replaces a genuine many-body effect with a single-particle description. A strong experimental effort has been performed in order to check both models in the last few years.[86, 106–114]

A different phenomenological approach, known as interacting superparamagnetic model (ISP) have been proposed and represents a further step in the full comprehension of these systems.[63] This theory has been applied successfully to Co nanoparticles on a Cu matrix,[63] both silver-encapsulated[115] and silica-encapsulated iron nanoparticles[116] and, more recently, in Ref. [117]. More recently, another model was proposed to explain the transition from the superparamagnetic to the blocked state in interacting nanoparticles. The proposed model considers a simple modification of the random anisotropy model (RAM) taking into account the concentration and size of the nanoparticles, as well as the field dependence of the magnetic correlation length.[118] By doing so a quantitative analytical expression relating individual and collective properties of nanoparticle systems was obtained for a wide range of concentrations.[118] Such a model was already tested with success in different nanoparticle systems.[40, 118, 119]

It is worth mentioning that, despite the theoretical approach to be employed, the experimental challenge is the precise control of several parameters, such as the crystalline structure, shape, concentration, size distribution and chemical composition of the nanoparticles and the matrix. A continuous effort has been made in this direction and important results have been achieved.[120–125] Once the nanograins are obtained with a good chemical stability and rather narrow size distribution, one can easily control the intensity of the dipolar interactions among the nanoparticles by different dispersions (with different concentrations) in a non-metallic matrix such as a polymer or paraffin.[49, 79] Examples of such experiments will be given below.

As a matter of fact, usually the samples do not follow the classical scaling law of superparamagnetism.[62] The observed deviations are frequently attributed to single-particle blocking effects and/or to random collective interactions among particles. It is worth noting that such discrepancies occur even at rather high temperatures, where single-particle blocking effects should be negligible. Although some samples indeed display a superparamagnetic-like behaviour, the fitting parameters are spurious. In fact, the results obtained from conventional fitting procedures turn out to be unrealistic, as clearly demonstrated by Monte Carlo simulations in a system of Co nanoparticles with dipolar interactions.[53] Such behaviour has been attributed to the failure of conventional models to include either the effect of magnetic interactions[63] and/or the temperature dependence of the anisotropy constant.[126] It is worth stressing that extreme care must be taken when magnetic moment values are inferred from magnetization measurements. Indeed, spurious results can appear as a consequence of magnetic interactions among nanoparticles and/or from the inadequacy of the Langevin approach to treat systems with rather high magnetic anisotropy. In other words, when magnetic interactions are present, a careful analysis has to be done in order to obtain reliable results.

An overview of recent models on magnetic interactions among nanoparticles will be given below, with some examples of applications in different magnetic systems.

4.1. Interacting Superparamagnetic Model

As previously mentioned, the development of analytical theories to describe the dipole–dipole interaction in randomly oriented granular magnetic systems is not an easy task. Empirical models have rapidly evolved to describe the hysteretic[48] and anhysteretic[63] properties of a system composed of superparamagnetic grains that mutually interact by means of magnetostatic fields. These theories are based on a sort of mean field caused by the presence of neighboring magnetic particles, which, depending on the field application procedure, can act as a magnetizing field (giving rise to hysteresis), or as an additional torque, which can be properly taken into account by adding a phenomenological temperature T^* to the real temperature (resulting in an apparent temperature, $T_a = T + T^*$).[63]

The role of this additional temperature T^* is to introduce a disorder of the magnetic moments, caused by the random dipolar field acting on each dipole, changing in direction, sign, and magnitude at a very high rate[127] (of the order of 10^9 Hz). Thus, T^* is not an arbitrary quantity, but it is related to the *rms* dipolar energy ε_D throughout the relation $kT = \varepsilon_D$, where $\varepsilon_D = \alpha\mu^2/d^3$, d is the mean interparticle distance and α is a constant derived from the sum of all dipolar energy contributions.[128, 129] Using $Nd^3 = 1$, where N is the number of particles per unit of mass and $M_S = N\mu$, M_S being the saturation magnetization, T^* can be expressed in an alternative form:

$$T^* = (\alpha N/k_B)\langle\mu\rangle^2 = \alpha M_s^2/k_B N \qquad (49)$$

Delivered by ingenta to: Boulder Labs Library IP : 132.163.150.249 Mon, 11 Aug 2008 19:50:43

REVIEW

The ISP model considers dipolar interactions as a perturbation of the superparamagnetic regime. In this way, interaction effects are taken into account by adding the phenomenological temperature T^* to the real temperature in the Langevin function (Eq. 19):

$$M(H,T) = N\int_0^\infty \mu L\left(\frac{\mu H}{k_B(T+T^*)}\right) f(\mu)\, d\mu \qquad (50)$$

Because the hysteresis loops can be usually fitted using a conventional Langevin function, one can relate the obtained parameters, which are called *apparent*, with the real ones, μ and N:

$$\mu_{app} = \left(\frac{1}{1+T^*/T}\right)\mu \qquad (51)$$

$$N_{app} = \left(1+\frac{T^*}{T}\right)N \qquad (52)$$

The α and N values can be determined by fitting the low field susceptibility $\chi(T) = \partial M(H,T)/\partial H$:

$$\frac{\rho}{\chi(T)} = 3k_B N\left(\frac{T}{M_s^2}\right) + 3\alpha \qquad (53)$$

where ρ is defined as the ratio:[63]

$$\rho = \frac{\langle\mu^2\rangle}{\langle\mu\rangle^2} = \frac{\langle\mu_{app}^2\rangle}{\langle\mu_{app}\rangle^2} \qquad (54)$$

Following this procedure, one can obtain the true mean magnetic moment as a function of temperature (the detailed procedure is explained in Ref. [63]).

One of the main achievements of such approach is the elucidation of the existence of a rather interesting magnetic region, called interacting superparamagnetic regime (ISP). The ISP approach was extensively tested on Cu-Co granular alloys,[63] but in such metallic systems one cannot exclude the presence of RKKY-like interactions among the Co grains, fact that would hinder the real effects of dipolar interactions. In order to overcome this difficulty, and to test the validity of the model in other systems, the ISP model was tested in two different granular systems: one consisting of cobalt nanoparticles immersed in a SiO_2 matrix, prepared by co-sputtering,[117, 130] and another one consisting of iron nanoparticles produced by chemical routes. For the Co-SiO_2 system, the values of μ obtained through the ISP model gave the right tendency, but with values slightly above those calculated from the diameter obtained from TEM images.[117] This difference was attributed to several reasons, one of which being that, due to the rather high metallic concentration, interactions can be strong enough to make the assumptions of the ISP model no longer valid. Also, other instrinsic parameters, such as the rather wide distribution of particle sizes could also influence the analysis of the data, and therefore better samples would be necessary to make a more detailed study of the ISP regime.

In fact, a system formed by colloidal nanoparticles embedded into a nonmagnetic polymer is an interesting framework to systematically study the effect of the dipolar interaction, by varying the concentration of the nanoparticles. Such idea was employed to study the magnetic response of magnetite nanoparticles (mean size of 7 nm) coated by surfactant molecules dispersed in paraffin in different concentrations.[131] The dilution used in that work were 0.05, 0.5, 5, and 45% mass colloid/mass of paraffin ratios, respectively, hereinafter named C005, C05, C5 and C45, respectively. Zero-field-cooling and field-cooling magnetization curves were found to be extremely sensitive to the effect of the interactions. As can be clearly seen in Figure 8, for increasing particle concentration the splitting points between ZFC and FC curves as well as the maxima of the ZFC curves shift to higher temperatures, indicating an increase in the effective energy barrier. A similar trend was previously observed by Dormann et al. and in Monte Carlo simulations.[67, 96, 132]

Delivered by Ingenta
Boulder Labs Library
IP : 132.163.129.249
Mon, 11 Aug 2008 19:50:43

M versus H loops taken at different temperatures were fitted simultaneously for the as-prepared (powder), C45 and C5 samples. The fittings were quite good in all cases,[131] but, as previously mentioned, good fits using a distribuition of Langevin functions are not surprising, but often the obtained size distribution parameters are quite different from those obtained through structural studies. However, by using the ISP model, the fitting results from magnetic data agreed quite well with the available

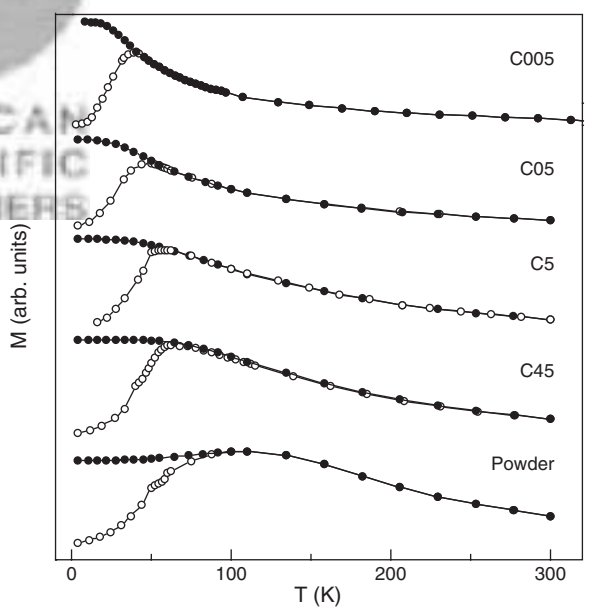

Fig. 8. ZFC-FC magnetization measurements of magnetite nanoparticles with different concentrations. Blocking temperatures shift towards higher temperatures when nanoparticle concentration increases. FC curves in the irreversibility region qualitatively show the intensity of the interaction. It increases when dipolar interaction increases. Reprinted with permission from [131], J. M. Vargas et al., *Phys. Rev. B* 72, 184428 (**2005**). © 2005, American Physical Society.

structural parameters.[131] The temperature T^* was found to decrease when T increases, as expected.

4.2. Effect of Interactions on the Blocking Temperature

Although for high concentrations of magnetic nanoparticles there is no doubt that nanoparticle blocking processes are not independent,[133] there are some discussions about the existence of spin glass-like or magnetic order in such systems. However, many results claimed that the existence of collective freezing or magnetic order is explained by progressive blocking of independent particles.[134–136] From the applications viewpoint, the understanding of the collective behavior resulting from interactions can be very important in the development of new magnetic devices, because in applications such as high-moment soft magnetic materials, magnetic sensors, and improved nanocomposite magnets, the required volume fraction of nanoparticles goes into the strong interaction regime. In this section we introduce a new model which can give important contributions to the study of collective behavior and other fundamental questions of nanoparticle systems.

The effect of external magnetic field on the blocking temperature has been considered for uniaxial magnetic systems by several authors.[137, 138] The simple analytical expression usually employed is:

$$T_B(H) = \frac{KV}{25k_B}\left[1 - \left(\frac{H}{H_k}\right)\right]^{\alpha} \quad (55)$$

where the exponent α is usually close[139] to 1.5. Figure 9 shows the temperature dependence of ZFC and FC magnetization measured for a $Co_{0.45}(SiO_2)_{0.55}$ sample measured at different applied fields. The derivative

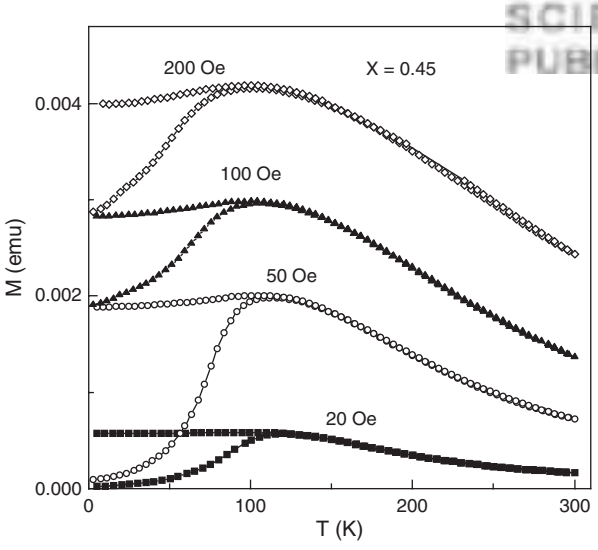

Fig. 9. FC and ZFC magnetization curves measured for $Co_x(SiO_2)_{1-x}$ samples with $x = 0.45$ for different values of applied magnetic field. Reprinted with permission from [83], W. C. Nunes et al., *Phys. Rev. B* 72, 212413 **(2005)**. © 2005, American Physical Society.

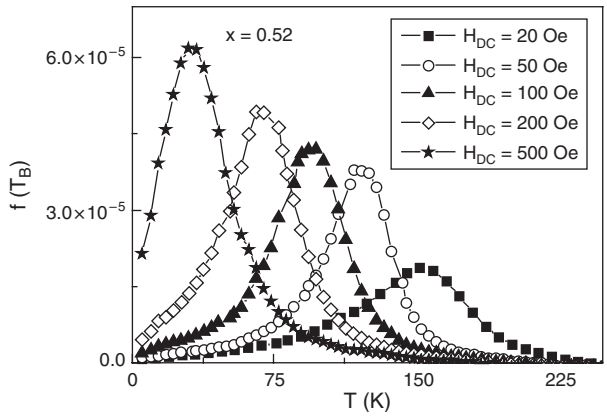

Fig. 10. Blocking temperature distribution obtained from ZFC and FC magnetization curves measured for different applied fields in the $Co_{0.52}(SiO_2)_{0.48}$ sample. Reprinted with permission from [83], W. C. Nunes et al., *Phys. Rev. B* 72, 212413 **(2005)**. © 2005, American Physical Society.

Delivered by Ingenta to:
Boulder Labs Library
IP : 132.163.150.253
Mon, 11 Aug 2009 19:50:45

$d[M_{FC} - M_{ZFC}]/dT$ was used to estimate the distribution of blocking temperatures $f(T_B)$, and its corresponding mean value, as described in Section 3. The calculated distributions for a $Co_{0.52}(SiO_2)_{0.48}$ sample at different applied fields are shown in Figure 10.

Equation (55) was used to fit the field dependence of blocking temperature of $Co_x(SiO_2)_{1-x}$ samples for three different Co concentrations x (the same samples analyzed in Section 3.4), see Figure 11. The fitting results of Eq. (55) to $T_B(H)$ lead to a particle size much larger than the one estimated by SAXS measurements,[118] but, on the other hand, the K_{eff} values estimated through the fit turned out to be well below those of bulk Co.[118] As a matter of fact, one can conclude that the conventional SP model is not a good approach to describe the magnetic behaviour of the more concentrated samples, as was also observed in analysis of the ZFC and FC curves and hysteresis loops. All the features inferred by the application of the conventional superparamagnetic approach (i.e., lower k_{eff}, larger Λ (effective volume) and T_B values, respectively) suggest the existence of coupling between particles, which

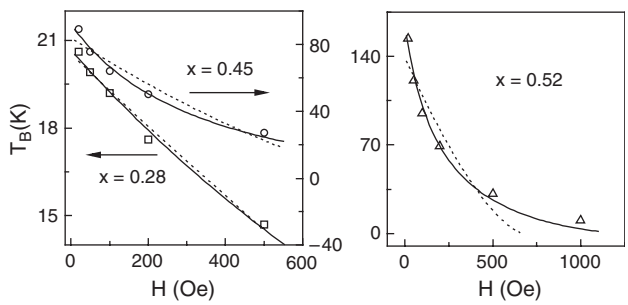

Fig. 11. Field dependence of the blocking temperature for three different concentrations of $Co_x(SiO_2)_{1-x}$ samples. Fits were done by using Eq. (55) (dashed line) and the modified RAM model, given by Eq. (60) (solid line). Reprinted with permission from [83], W. C. Nunes et al., *Phys. Rev. B* 72, 212413 **(2005)**. © 2005, American Physical Society.

can be considered using a modified random anisotropy model (RAM). According to this model, the anisotropy is averaged to an effective value K_{eff} within the correlation length due to the magnetic interactions, whose magnitude decreases when the correlation length increases due to a statistical random walk effect. Thus, for N coupled particles, the relevant parameters for the magnetization processes are given by $K_{\text{eff}} = K/N^{1/2}$, $\Lambda = VN$, and $T_{\text{B}} = K_{\text{eff}} V_{\text{eff}} = N^{1/2} KV$. This model was originally developed to explain the magnetic properties of amorphous ferromagnets (and afterwards soft nanocrystals embedded in a ferromagnetic matrix)[140–142] and, consequently, modifications are required if one wishes to apply it to nanoparticles dispersed in a nonmagnetic matrix, basically taking into account the volume fraction x of nanoparticles. Two simple modifications of the RAM expressions for K_{eff} and V_{eff} that account for above mentioned points are

$$K_{\text{eff}} = k/\sqrt{N}; \quad \Lambda = \frac{\pi}{6}[D + x(L^3 - D^3)] \tag{56}$$

where N is the number of correlated particles, and D is their diameter, i.e.,

$$N = [1 + x(L^3 - D^3)/D^3] \tag{57}$$

Both expressions tend, respectively, to the anisotropy and volume of an individual particle when interactions are very weak and $L \to D$; on the other hand, when $L \gg D$, they tend to the usual relations used in the study of correlated nanoparticle systems. Michels et al.[143] evidenced, by means of small-angle neutron scattering, that the correlation length of Ni and Co electrodeposited nanocrystals decreases with increasing applied field. This result is reasonable, since L is a measure of the average distance over which magnetization fluctuations are correlated. The experimentally observed correlation length can be expressed as a function of the applied field as

$$L_H = D + \sqrt{\frac{2A_{\text{eff}}}{M_{\text{S}}}} \tag{58}$$

where A_{eff} represents the interaction intensity which, for nanocrystalline alloys, is the intergranular exchange constant A.[144] Usually, the distribution of sizes and distances implies a distribution of the strength and the orientation of the interaction, which would rather lead to a "correlated superspin-glass-like" state.[115] In such case the use of the following expression is more effective:[143]

$$L_H = D + \sqrt{\frac{2A_{\text{eff}}}{M_{\text{S}}H + C}} \tag{59}$$

where the parameter C assumes a value that is not totally arbitrary, but it is related to the *rms* strength of the dipolar interaction. One expects the parameter C to be close to zero for systems of particles clustered together and to increase with the progressive dilution of particles, reaching a value $C \approx 2A_{\text{eff}} - M_{\text{S}}H$ for a system composed of non-interacting particles.[118]

By substituting the anisotropy and volume of individual particles of Eq. (53) by the effective anisotropy and particle volume, respectively, one can calculate the field dependence of the blocking temperature for coupled particles in terms of the structural parameters of nanoparticulate systems:

$$T_{\text{B}} = \frac{K\pi[D^3 + x(L_H^3 - D^3)]}{6 \times 25 k_{\text{B}}[1 + x(L_H^3 - D^3)/D^3]^{1/2}} \times \left[1 - \left(\frac{H_{\text{DC}} M_{\text{S}}[1 + x(L_H^3 - D^3)/D^3]^{1/2}}{2K}\right)\right]^{1.5} \tag{60}$$

Equation (60) was employed to fit the experimental data of Figure 11, with L_H given by Eq. (59). The fits, represented by the solid lines, were carried out by using the experimental D values (previously estimated by SAXS[115]), $M_{\text{S}} = 1420$ erg/cm^3 (the bulk Co value), and $A = 3.1 \times 10^{-7}$ erg/cm^1, and K and C as free parameters. Equation (59) provides a very good description of the field dependence of T_{B} for all samples by employing K_{eff} values of the order of magnitude of the bulk anisotropy of Co and in agreement with its expected particle size dependence.[145] Furthermore, the C values employed in the fit lead to L_0, that is L_H for zero applied field, values that are consistent with its expected concentration dependence, i.e., they increase with increasing Co concentration.[118]

Many results suggest that it is possible to indirectly detect the formation of a collective magnetic state arising from the dipolar interactions among individual particles.[41] Such magnetic ordering has been called "superferromagnetism" in cases where the dipolar interaction leads to ferromagnetic-like coupling among the magnetic entities.[103] The compact array of nanoparticles leads to a ferromagnetic coupling among the nanoparticles, however the correlation length due to the interaction is still quite short around the blocking temperature. This explains why the properties can still be reasonably described in the framework of independent "particle clusters," after a renormalization that takes into account the correlation length. Furthermore, such renormalization approach can be applied to the thermal demagnetization process from a saturated state where individual relaxation must also take place, because the field dependence of correlation length is considered.

In the case of the 2D arrays, the rather organized arrangement of the self-assembled nanoparticles reduces the complications introduced by positional randomness, typical of other nanoparticle systems, such as granular solids. Moreover, these systems provide an excellent setting for studying the influence of the collective behavior of nanoparticles on the magnetization process. The study was performed in samples containing 2D arrays (prepared

Delivered by Ingenta to: Boulder Labs Library IP: 132.163.4.249 Mon, 11 Aug 2008 19:50:43

AMERICAN SCIENTIFIC PUBLISHERS

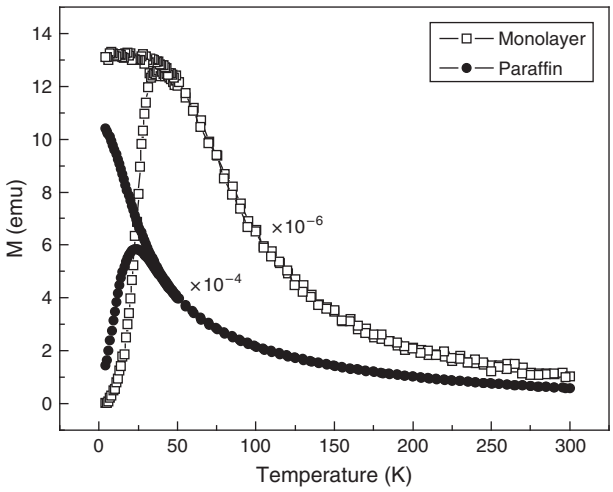

Fig. 12. ZFC and FC magnetization curves, measured under a field of 20 Oe for both monolayer sample and diluted nanoparticles of γ-Fe_2O_3, respectively. Reprinted with permission from [40], M. Knobel et al., *J. Non-Cryst. Sol.* 353, 743 **(2007)**. © 2007, Elsevier.

Delivered by Ingenta to:
Boulder Labs Library
IP : 132.163.4.102
Mon, 11 Aug 2008 19:59:15

by Langmuir–Blodgett technique, LB) and 3D (by dilution in paraffin wax solid solution) dispersions of colloidal iron oxide nanoparticles.[40]

Figure 12 shows the ZFC and FC magnetizations (as an example, measured under applied field of 20 Oe) for the samples in which the Fe_3O_4 NPs are diluted in paraffin wax forming a solid solution and in a LB film, respectively. The distribution of T_B and the mean blocking temperature $\langle T_B \rangle$ were calculated by the derivative of the curve resulted from the difference between the M_{FC} and M_{ZFC} magnetization for several values of applied magnetic fields H. The field dependence of $\langle T_B \rangle$ is shown in Figure 13 for both studied samples. The magnetic properties of these samples were analyzed by using the nanoparticles coupling model (Eqs. (58) to (60)). In order to obtain the values of M_S and K of the nanoparticles, the T_B versus H curve of diluted sample was fitted by using the superparamagnetic description, Eq. (55), and average particles diameter obtained through TEM.

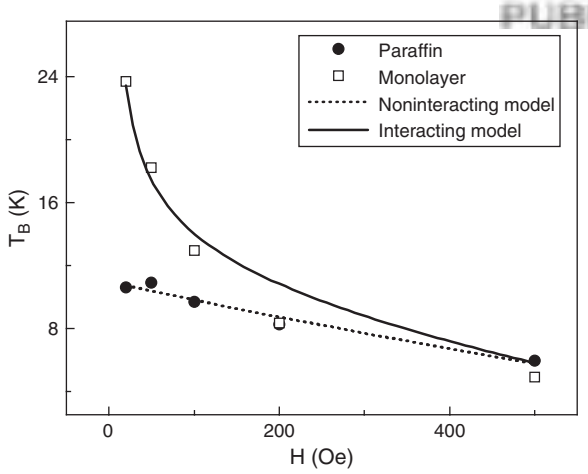

Fig. 13. Field dependence of the blocking temperature for both monolayer sample and diluted nanoparticles of γ-Fe_2O_3. Fits using Eq. (55) (dashed-dotted line) and the modified RAM expression, given by Eq. (60) (solid line). Reprinted with permission from [40], M. Knobel et al., *J. Non-Cryst. Sol.* 353, 743 **(2007)**. © 2007, Elsevier.

The dashed line in Figure 13 is the result of the best fit to the Eq. (55), by using $\alpha = 1.5$, K and M_S as free parameters and the particle diameter $D = 5.8$ nm (extracted from TEM images). Both M_s and K obtained from the fit agree rather well with the values usually observed in iron oxide NPs.[79]

It is worth noting that the $\langle T_B \rangle$ versus H behaviour of NPs forming a 2D array is quite different from the diluted 3D sample. The T_B of the LB film has a good agreement with the noninteracting model only at high applied fields; at low fields, T_B shows a sharp increase. This result suggests the formation of a collective magnetic state arising from the dipolar interactions among individual particles. In this case, the magnetic properties of the system are characterized by a cluster size given by the correlation length that is field dependent, see Eqs. (59) and (60). As a consequence, a collective reversal of the magnetic moment of the nanoparticles in the LB film may occur, leading to higher blocking temperatures for lower applied fields. However, under a higher applied magnetic field an individual reversal of particle magnetic moment arises, as in the diluted NPs sample (Fig. 13). In other words, the size of the cluster of monolayer sample decreases with the applied field, reaching the diameter of the individual nanoparticle when the applied field overcomes the dipolar interaction field, as expected.[118] As a matter of fact, the interacting model provides a very good description of the field dependence of T_B also in the case of 2D array, leading to rough estimates of A_{eff} due to dipolar interaction.[40]

5. THE ROLE OF THE SURFACE

As previously mentioned, surface effects can be very important in systems of nanoparticles. With decreasing particle size, the fraction of atoms that lies near or on the surface increases, making the surface effect more and more important. It is estimated that in a 3 nm diameter particle 80% are surface atoms.[2, 146] Also, surface effects can be observed not only on small particles, but also in larger particle systems, depending on the chemical composition of the nanoparticles, their crystalline state, among other intrinsic parameters.

The surface effects result basically from the break of symmetry of the lattice at the surface of the particles,[45, 147, 148] which leads to site-specific surface anisotropy of unidirectional character, from the broken exchange bonds. The low coordination number on the particle surface affects the magnetic behaviour on the surface and could propagate within the particle. Such influence can manifestate strongly or weakly, mainly depending

on the temperature at which the experiment is made. For instance, some experiments[149, 150] and Monte Carlo calculations[151] show that the Curie temperature decreases with decreasing particle size. Therefore, the magnetization near and on the surface is lower than the in the core of the nanoparticle. This effect was indeed reported in magnetization measurements of γ-Fe_2O_3 nanoparticles.[152] High-field magnetization measurements of γ-Fe_2O_3 (Ref. [152]) and Co (Ref. [153]) show an increasing of nonsaturation tendency for small particle sizes. High-field open hysteresis loops were observed, and they were attributed to the high surface anisotropy. High field magnetic relaxation of a sping-glass-like surface state was observed in Ni-ferrite particles.[154, 155]

Many of the systems that exhibit surface effects could be described by a core–shell model.[60, 98, 148, 155] This model considers each particle as composed of internal magnetic ordered core (with ferro- or antiferromagnetic ordering), that can be described by the Stoner-Wohlfarth relaxation model; and a disordered shell of spins, that interact among them and the particle core. This model satisfactorily describes the observed features in magnetization measurements of ferromagnetic-like[60, 98] (FeNiB and CoNiB nanoparticles) and antiferromagnetic-like systems[156] (NiO). At high temperatures two contributions to the magnetization are observed on the $M(H)$ curves, one superparamagnetic-like, that saturates according the Langevin law, and another one that does not saturates and displays a linear behavior, associated with the external shell. When lowering the temperature a strong increment on the magnetization value is observed, product of the ordering of magnetic surface spin in small clusters due to the short range coupling. At low temperatures, near 7 K, the ZFC curve shows a maximum, while the FC curve increases noticeably.[60] The hysteresis loops show an anomalous shape on this temperature regime (near and above 7 K), that leads to unexpected coercive field and remanent magnetization behaviour. In addition, time relaxation measurements show, at low temperatures (near 7 K), two components,[60, 98] which reflects in a pronounced step on the thermal viscosity. All experimental data have been reproduced and interpreted within the core–shell model by Monte Carlo simulations. When the temperature is lowered, magnetic clusters grow, increasing the total magnetization. At low temperatures the effective anisotropy is strongly increased due to surface anisotropy on the surface clusters. The thermal effect becomes less important, leading to the competition between the local surface anisotropy and the ferromagnetic short-range interaction. Such competition originates a glass like behaviour that manifest itself on the ZFC-FC and hysteresis measurements. Ferromagnetic Resonance studies performed on this FeNiB, CoNiB and NiO systems also reflect the surface effects.[156] The experimental results show a strong increment of the effective linewidth at low temperatures due to the surface anisotropy. In addition, the resonance field falls with the increment of the magnetization, owing to the polarization of the core by surface clusters. Thus, the field necessary to get the resonance condition becomes smaller than expected.

For small nanoparticles the surface effect must be considered to estimate the size dependence of the effective anisotropy, presented in Section 2. Usually, it has been considered as an effective anisotropy term given approximately by the following phenomenological expression:

$$K_{\text{eff}} = K_V + \frac{6}{\langle D \rangle} K_S \tag{61}$$

Such expression has been extensively applied in to take into account the effect of the surface on nanostructured systems, with rather good success in most of the cases. In fact, surface effects can be important even when dealing with bigger particles, and a careful analysis is necessary to properly separate the effects of structural disorder, interparticle interactions and surface contributions.

Delivered by Ingenta
Boulder Labs Library
IP: 132.163.130.249
Mon, 11 Aug 2008 15:50:45

6. CONCLUSIONS

A brief review on the basic concepts and experimental techniques related to granular magnetic nanostructures was presented, with emphasis in a rather didactic presentation. The transition from ideal model systems to real ones was gradually introduced, by taking into account the effect of the distribution of grain sizes and the important role played by the surface, mainly in very small nanoparticles. Also, a discussion on the role of magnetic interaction, mainly of dipolar origin, was presented, and an overview of recent models that consider such intricate interparticle interactions were discussed with some detail. It is worth mentioning that a full understanding of the magnetic properties of granular systems is still far from being complete, and many challanges need yet to be overcome in this fascinating research field.

Acknowledgments: The authors thank Brazilian agencies FAPESP and CNPq for financial support, and the Laboratório Nacional de Luz Síncrotron (LNLS) for the use of Laboratório de Microscopia Eletrônica (TEM facilities) and SAXS beamline. We are grateful to Dr. P. Allia, P. Panissod, R. Zysler, and A. Bakuzis for fruitful discussions.

References and Notes

1. G. C. Hadjipanayis and G. A. Prinz (eds.), Science and Technology of Nanostructured Magnetic Materials, Series B: Physics, Plenum Press, New York, NATO Advanced Study Institute **(1991)**, Vol. 259.
2. J. L. Dormann and D. Fiorani (eds.), Magnetic Properties of Fine Particles, North-Holland, Amsterdam **(1992)**.
3. H. J. Lee and S. H. Jeong, *Textile Research Journal* 75, 551 **(2005)**.
4. R. H. Müller, S. Runge, V. Ravelli, W. Mehnert, A. F. Thünemann, and E. B. Souto, *Int. J. Pharm.* 317, 82 **(2006)**.

5. E. D. Kuempel, C. L. Tran, and V. Castranova, *Inhalation Toxicology* 18, 717 (**2006**).
6. A. Jordan, R. Scholz, and K. Maier-Hauff, F. K. H. van Landeghem, N. Waldoefner, U. Teichgraeber, J. Pinkernelle, H. Bruhn, F. Neumann, B. Thiesen, A. von Deimling, and R. Felix, *J. Neuro-Oncology* 78, 7 (**2006**).
7. M. N. Baibich, Magnetism, Magnetic Materials and Their Applications, edited by F. Leccabue and V. Sagredo, World Scientific, Singapure (**1996**), pp. 69–80.
8. P. H. Shingu (ed.), *Mechanical alloying, Proceedings of the 1st International Symposium on Metastable, Mechanically Alloyed and Nanocrystalline Materials* (**Kyoto 1991**), Materials Science Forum, Singapore (**1992**), Vol. 88–90.
9. M. G. M. Miranda, G. J. Bracho Rodríguez, A. B. Antunes, M. N. Baibich, E. F. Ferrari, F. C. S. da Silva, and M. Knobel, *J. Magn. Magn. Mater.* 185, 331 (**1998**).
10. P. Allia, M. Knobel, P. Tiberto, and F. Vinai, *Phys. Rev. B* 52, 15398 (**1995**).
11. S. Mørup and E. Tronc, *Phys. Rev. Lett.* 72, 3278 (**1994**).
12. J. Garcia-Otero, A. J. Garcia-Bastida, and J. Rivas, *J. Magn. Magn. Mater.* 189, 337 (**1998**).
13. C. L. Chien, *J. Appl. Phys.* 69, 5267 (**1991**).
14. A. Hütten and G. Thomas, *Ultramicroscopy* 52, 581 (**1993**).
15. A. Lopez, F. J. Lazaro, R. Von Helmolt, J. L. Garcia-Palacios, J. Wecker, and H. Cerva, *J. Magn. Magn. Mater.* 187, 221 (**1998**).
16. J. L. Dormann, R. Cherkaoui, L. Spinu, M. Noguhs, F. Lucari, F. D'Orazio, D. Fiorani, A. Garcia, E. Tronc, and J. P. Jolivet, *J. Magn. Magn. Mater.* 187, L139 (**1998**).
17. J. R. Childress and C. L. Chien, *Phys. Rev. B* 43, 8089 (**1991**).
18. J. Nogues, J. Sort, and V. Langlais, *International Journal of Nanotechnology* 2, 23 (**2005**).
19. D. Fiorani, L. Del Bianco, and A. M. Testa, *Phys. Rev. B* 73, 092403 (**2006**).
20. J. A. De Toro, J. P. Andres, and J. A. Gonzalez, *Phys. Rev. B* 73, 094449 (**2006**).
21. G. Malinowski, M. Hehn, and P. Panissod, *J. Phys.-Conseded Matter* 18, 3385 (**2006**).
22. K. Theis-Brohl, M. Wolff, and A. Westphalen, *Phys. Rev. B* 73, 174408 (**2006**).
23. K. B. Li, Y. H. Wu, and G. C. Han, *Thin Solid Films* 505, 22 (**2006**).
24. M. Doi, M. Izumi, H. Endo, H. N. Fuke, H. Iwasaki, and M. Sahashi, *IEEE Trans. Magn.* 41, 2932 (**2005**).
25. D. Morecroft, J. L. Prieto, and M. G. Blamire, *J. Appl. Phys.* 97, 10C518 (**2005**).
26. S. H. Jang, T. Kang, H. J. Kim, and K. Y. Kim, *J. Magn. Magn. Mater.* 240, 192 (**2002**).
27. C.-L. Lee, J. Kools, A. J. Devasahayam, M. Mao, and C.-C. Hu, *J. Magn. Magn. Mater. (Special Issue)* 286, 200 (**2005**).
28. J. Wang, H. L. Duan, Z. P. Huang, and B. L. Karihaloo, *Proceedings of The Royal Society A-Mathematical Physical and Engineering Sciences* 462, 1355 (**2006**).
29. A. I. Morosov and A. S. Sigov, *Phys. Solid State* 46, 395 (**2004**).
30. M. N. Baibich, J. M. Broto, A. Fert, F. Nguyen van Dau, F. Petroff, P. Etienne, G. Creuzet, A. Friederich, and J. Chazeles, *Phys. Rev. Lett.* 61, 2472 (**1988**).
31. S. Mitani, H. Fujimori, and S. Ohnuma, *J. Magn. Magn. Mater.* 177–181, 919 (**1998**).
32. J. C. Denardin, M. Knobel, X. X. Zhang, and A. B. Pakhomov, *J. Magn. Magn. Mater.* 262, 15 (**2003**).
33. A. L. Brandl, J. C. Denardin, L. M. Socolovsky, M. Knobel, and P. Allia, *J. Magn. Magn. Mater.* 272–276, 1526 (**2004**).
34. D. Kechrakos and K. N. Trohidou, *Phys. Rev. B* 71, 054416 (**2005**).
35. H. Endo, Y. Kado, M. Mitsuishi, and T. Miyashita, *Macromolecules* 39, 5559 (**2006**).
36. K. Lambert, L. Wittebrood, I. Moreels et al., *J. Colloid Interface Sci.* 300, 597 (**2006**).
37. Y. Fujiki, N. Tokunaga, S. Shinkai, and K. Sada, *Angew. Chem. Int. Ed.* 45, 4764 (**2006**).
38. K. L. Genson, J. Holzmueller, C. Jiang, J. Xu, J. D. Gibson, E. R. Zubarev, and V. V. Tsukruk, *Langmuir* 22, 7011 (**2006**).
39. Y. J. Shen, Y. L. Lee, and Y. M. Yang, *J. Phys. Chem. B* 110, 9556 (**2006**).
40. M. Knobel, W. C. Nunes, H. Winnischofer, T. C. R. Rocha, L. M. Socolovsky, C. L. Mayorga, and D. Zanchet, *J. Non-Cryst. Sol.* 353, 743 (**2007**).
41. J. C. Denardin, A. L. Brandl, M. Knobel, P. Panissod, A. B. Pakhomov, H. Liu, and X. X. Zhang, *Phys. Rev. B* 65, 64422 (**2002**).
42. W. Shih, *Phys. Rev.* 38, 2051 (**1931**).
43. C. Elmore, *Phys. Rev.* 54, 309 (**1938**).
44. C. Kittel, *Phys. Rev.* 70, 965 (**1946**).
45. L. Néel, *C. R. Acad. Sci., Paris* 228, 664 (**1949**); L. Néel, *Ann. Geophys.* 5, 99 (**1949**).
46. B. D. Cullity (ed.), Introduction to Magnetic Materials, Addison-Wesley Publishing Co., Reading, Massachusetts (**1972**).
47. P. Bean and J. D. Livingston, *J. Appl. Phys.* 30, 120 (**1959**).
48. P. Allia, M. Coisson, M. Knobel, P. Tiberto, and F. Vinai, *Phys. Rev. B* 60, 12207 (**1999**).
49. J. M. Vargas, C. Ramos, R. D. Zysler, and H. Romero, *Physica B* 320, 178 (**2002**).
50. E. C. Stoner and E. P. Wohlfarth, *Phil. Trans. Roy. Soc. A* 240, 599 (**1948**); Reprinted by *IEEE Trans. Magn.* 27, 3475 (**1991**).
51. M. El Ghannami, C. Gómez-Polo, G. Rivero, and A. Hernando, *Europhys. Lett.* 26, 701 (**1994**).
52. J. L. Dormann, F. D'Orazio, F. Lucari, E. Tronc, P. Prenè, J. P. Jolivet, D. Fiorani, R. Cherkaoui, and M. Nogués, *Phys. Rev. B* 53, 14291 (**1996**).
53. M. El-Hilo, R. W. Chantrell, and K. O'Grady, *J. Appl. Phys.* 84, 5114 (**1998**).
54. G. Szabó and G. Kádár, *Phys. Rev. B* 58, 5584 (**1998**).
55. D. Kechrakos and K. N. Trohidou, *Phys. Rev. B* 58, 12169 (**1998**).
56. J. M. González, O. A. Chubykalo, and J. Gonzáles, *Phys. Rev. B* 55, 921 (**1997**).
57. M. Knobel, E. F. Ferrari, and F. C. S. da Silva, *Mater. Sci. Forum* 302–303, 169 (**1999**).
58. R. Iglesias, H. Rubio, and S. Suárez, *Appl. Phys. Lett.* 73, 2503 (**1998**).
59. J. d'Albuquerque e Castro, D. Altbir, J. C. Retamal, and P. Vargas, *Phys. Rev. Lett.* 88, 237202 (**2002**).
60. E. De Biasi, C. A. Ramos, R. D. Zysler, and H. Romero, *Phys. Rev. B* 71, 104408 (**2005**).
61. H. Mamiya, I. Nakatani, T. Furubayashi, and M. Ohnuma, *Trans. Magn. Soc. Japan* 2, 36 (**2002**).
62. A. L. Brandl, J. C. Denardin, L. M. Socolovsky, M. Knobel, and P. Allia, *J. Magn. Magn. Mater.* 272–276, 1526 (**2004**).
63. P. Allia, M. Coisson, P. Tiberto, F. Vinai, M. Knobel, M. A. Novak, and W. C. Nunes, *Phys. Rev. B* 64, 144420 (**2001**).
64. J. C. Denardin, M. Knobel, L. S. Dorneles, and L. F. Schelp, *J. Magn. Magn. Mater.* 294, 206 (**2005**).
65. E. F. Ferrari, F. C. S. Silva, and M. Knobel, *Phys. Rev. B* 56, 6086 (**1997**).
66. J. M. Vargas, C. Ramos, R. D. Zysler, and H. Romero, *Physica B* 320, 178 (**2002**).
67. J. L. Dormann, D. Fiorani, and E. Tronc, *Adv. Chem. Phys.* 98, 283 (**1997**).
68. L. Spinu, C. J. O'Connor, and H. Srikanth, *IEEE Trans. Magn.* 37, 2188 (**2001**).
69. L. Spinu, H. Srikanth, A. Gupta, X. W. Li, and G. Xiao, *Phys. Rev. B* 62, 8931 (**2000**).
70. L. Spinu, H. Pham, C. Radu, J. C. Denardin, I. Dumitru, M. Knobel, L. S. Dorneles, and L. F. Schelp, *Appl. Phys. Lett.* 86, 012506 (**2005**).

Delivered by Ingenta to: Brunel Labs Library IP: 152.163.100.161 Mon, 11 Aug 2008 12:30:29

71. C. L. Chien, S. H. Liou, D. Kofalt, W. Yu, T. Egami, and T. R. McGuire, *Phys. Rev. B* 33, 3247 **(1986)**.
72. B. Window, *J. Phys. C: Metal Phys. C Supl.* 3, S323 **(1970)**.
73. L. M. Socolovsky and F. H. Sánchez, *Journal of Metastable and Nanocrystalline Materials* 22, 97 **(2004)**.
74. M. B. Fernández van Raap, L. M. Socolovsky, F. H. Sánchez, and I. Torriani, *J. Phys.: Condens. Matter* 14, 857 **(2002)**.
75. S. Mørup, Magnetic Microcrystals, in Applications of Mössbauer Spectroscopy, edited by R. L. Cohen, Academic Press, New York **(1980)**, Vol. II, p. 1.
76. R. W. Chantrell, M. El-Hilo, and K. O'Grady, *IEEE Trans. Magn.* 27, 3570 **(1991)**.
77. L. M. Socolovsky, F. H. Sánchez, and P. H. Shingu, *Physica B: Physics of Condensed Matter* 320, 149 **(2002)**.
78. W. C. Nunes, W. S. D. Folly, J. P. Sinnecker, and M. A. Novak, *Phys. Rev. B* 70, 014419 **(2004)**.
79. W. C. Nunes, F. Cebollada, M. Knobel, and D. Zanchet, *J. Appl. Phys.* 99, 08N705 **(2006)**.
80. G. Bertotti, Hysteresis in Magnetism, Academic Press, San Diego **(1998)**.
81. E. P. Wohlfarth, *J. Magn. Magn. Mater.* 39, 39 **(1983)**.
82. P. E. Kelly, K. O'Grady, P. I. Mayo, and R. W. Chantrell, *IEEE Trans. Magn.* 25, 3881 **(1989)**.
83. W. C. Nunes, L. M. Socolovsky, J. C. Denardin, F. Cebollada, A. L. Brandl, and M. Knobel, *Phys. Rev. B* 72, 212413 **(2005)**.
84. W. C. Nunes, E. De Biasi, C. Meneses, M. Knobel, H. Winnischofer, T. Rocha, D. Zanchet, *Appl. Phys. Lett.*, in press.
85. E. Vincent, J. Hamman, P. Prené, and E. Tronc, *J. Phys. I France* 4, 273 **(1994)**.
86. R. H. Kodama, *J. Magn. Magn. Mater.* 200, 359 **(1999)**.
87. T. Jonsson, J. Mattson, C. Djurberg, F. A. Khan, P. Nordlab, and P. Svendlindh, *Phys. Rev. Lett.* 75, 4138 **(1995)**.
88. C. Djurberg, T. Jonsson, P. Svendlinh, P. Nordlab, M. F. Hansen, F. Bodker, and S. Mørup, *Phys. Rev. Lett.* 79, 5154 **(1997)**.
89. D. Fiorani, J. L. Dormann, R. Cherkaoui, E. Tronc, F. Lucari, F. D'Orazio, L. Spinu, M. Nogues, A. García, and A. M. Testa, *J. Magn. Magn. Mater.* 196–197, 143 **(1999)**.
90. E. Bonetti, L. Del Bianco, D. Fiorani, D. Rinaldi, R. Caciuffo, and A. Hernando, *Phys. Rev. Lett.* 83, 2829 **(1999)**.
91. V. Skumryev, S. Stoyanov, Y. Zhang, G. Hadjipanayis, D. Givord, and J. Nogues, *Nature* 423, 19 **(2003)**.
92. M. El-Hilo, I. Bsoul, A. Rousan, and A. Hudeish, *J. Magn. Magn. Mater. (Part 1)* 272–276, 327 **(2004)**.
93. D. Kechrakos and K. N. Trohidou, *Phys. Rev. B* 62, 3941 **(2000)**.
94. Q. A. Pankhurst, D. H. Ucko, L. Fernández Barquín, and R. García Calderón, *J. Magn. Magn. Mater*. 266, 131 **(2003)**.
95. C. S. M. Bastos, M. Bahiana, W. C. Nunes, M. A. Novak, D. Altbir, P. Vargas, and M. Knobel, *Phys. Rev. B* 66, 214407 **(2002)**.
96. J. García-Otero, M. Porto, J. Rivas, and A. Bunde, *Phys. Rev. Lett.* 84, 167 **(2000)**; M. Porto, *J. Appl. Phys.* 92, 6057 **(2002)**.
97. L. M. Socolovsky, C. L. P. de Oliveira, J. C. Denardin, M. Knobel, and I. L. Torriani, *Physical Review B* 72, 184423 **(2005)**.
98. E. De Biasi, R. D. Zysler, C. A. Ramos, and H. Romero, *Physica B* 320, 203 **(2002)**.
99. D. A. Garanin and H. Kachkachi, *Phys. Rev. Lett.* 90, 065504 **(2003)**.
100. P. Allia, M. Coisson, J. Moya, V. Selvaggini, P. Tiberto, and F. Vinai, *Phys. Rev. B* 67, 174412 **(2003)**.
101. L. M. Socolovsky, C. L. P. Oliveira, J. C. Denardin, M. Knobel, and I. L. Torriani, *J. Appl. Phys.* 99 08C511 **(2006)**.
102. M. S. Hansen, C. B. Koch, and S. Mørup, *Phys. Rev. B* 62, 1124 **(2000)**.
103. M. F. Hansen and S. Mørup, *J. Magn. Magn. Matter.* 184, 262 **(1998)**.
104. J. L. Dormann, L. Bessais, and D. Fiorani, *J. Phys. C* 21, 2015 **(1998)**.
105. S. Mørup, *Eur. Lett.* 28, 671 **(1994)**.
106. O. Michele, J. Hesse, and H. Bremers, *J. Phys.-Condesed Matter* 18, 4921 **(2006)**.
107. J. L. Dormann, D. Fiorani, and E. Tronc, *J. Magn. Magn. Mater.* 202, 251 **(1999)**.
108. R. A. Borzi, S. J. Stewart, and G. Punte, *J. Magn. Magn. Mater.* 205, 234 **(1999)**.
109. M. Knobel, W. C. Nunes, and A. L. Brandl, *Phys. B-Condesed Matter* 354, 80 **(2004)**.
110. C. Papusoi, A. Stancu, and J. L. Dormann, *J. Magn. Magn. Mater.* 174, 236 **(1997)**.
111. F. Gazeau, E. Dubois, M. Hennion, R. Perzynski, and Yu. Raikher, *Europhys. Lett.* 40, 575 **(1997)**.
112. E. Tronc, P. Prené, J. P. Jolivet, J. L. Dormann, and J. M. Grenéche, *Hyperfine Interactions* 112, 97 **(1998)**.
113. J. L. Dormann, L. Spinu, E. Tronc, J. P. Jolivet, F. Lucari, F. D'Orazio, and D. Fiorani, *J. Magn. Magn. Mater.* 183, L255 **(1998)**.
114. R. D. Zysler, M. V. Mansilla, and D. Fiorani, *European Physical Journal B* 41, 171 **(2004)**.
115. C. Binns, M. J. Maher, Q. A. Pankhurst, D. Kechcrakos, and K. N. Trohidou, *Phys. Rev. B* 66, 184413 **(2002)**.
116. P. Tartaj, T. Gonzalez-Carreño, O. Bomati-Miguel, C. J. Serna, and P. Bonville, *Phys. Rev. B* 69, 94401 **(2004)**.
117. M. Knobel, W. C. Nunes, A. L. Brandl, J. M. Vargas, L. M. Socolovsky, and D. Zanchet, *Physica B: Physics of Condensed Matter* 354, 80 **(2004)**.
118. W. C. Nunes, L. M. Socolovsky, J. C. Denardin, F. Cebollada, A. L. Brandl, and M. Knobel, *Phys. Rev. B* 72, 212413 **(2005)**.
119. J. C. Denardin, W. C. Nunes, and M. Knobel, *Physica B* 384, 290 **(2006)**.
120. P. Poddar, T. Telem-Shafir, T. Fried, and G. Markovich, *Phys. Rev. B* 66, 60403 **(2002)**.
121. Z. Kaszkur, B. Mierzwa, and J. Pielaszek, *J. Appl. Crystall. (Part 2)* 38, 266 **(2005)**.
122. J. Gradl, H.-C. Schwarzer, F. Schwertfirm, M. Manhart, and W. Peukert, *Chem. Eng. Process. (Special Issue)* 45, 908 **(2006)**.
123. A. P. Chuklanov, S. A. Ziganshina, and A. A. Bukharaev, *Surf. Interface Anal.* 38, 679 **(2006)**.
124. T. O. Drews, M. A. Katsoulakis, and M. Tsapatsis, *J. Phys. Chem. B* 109, 23879 **(2005)**.
125. M. M. Oliveira, D. Ugarte, D. Zanchet, and A. J. G. Zarbin, *J. Colloid Interface Sci.* 292, 429 **(2005)**.
126. V. Franco and A. Conde, *J. Magn. Magn. Mater.* 277, 181 **(2004)**.
127. P. Allia, P. Tiberto, and F. Vinai, *J. Appl. Phys.* 81, 4599 **(1997)**.
128. A. H. Morrish, The Physical Principles of Magnetism, Wiley, New York **(1966)**.
129. C. Kittel, Introduction to Solid State Physics, Wiley, New York **(1968)**.
130. J. M. Vargas, L. M. Socolovsky, M. Knobel, and D. Zanchet, *Nanotechnology* 16, S285 **(2005)**.
131. J. M. Vargas, W. C. Nunes, L. M. Socolovsky, M. Knobel, and D. Zanchet, *Phys. Rev. B* 72, 184428 **(2005)**.
132. M. Bahiana, J. P. Pereira Nunes, D. Altbir, P. Vargas, and M. Knobel, *J. Magn. Magn. Matter.* 281, 372 **(2004)**.
133. S. Shtrikman and E. P. Wohlfarth, *Phys. Lett.* 85A, 467 **(1981)**.
134. Y. Sun, M. B. Salamon, K. Garnier, and R. S. Averback, *Phys. Rev. Lett.* 91, 167206 **(2003)**.
135. M. Sasaki, P. E. Jönsson, H. Takayama, and P. Nordblad, *Phys. Rev. Lett.* 93, 139701 **(2004)**.
136. E. P. Wohlfarth, *Phys. B+C* 86–88, 852 **(1977)**.
137. W. Wernsdorfer, E. B. Orozco, K. Hasselbach, A. Benoit, B. Barbara, N. Demoncy, A. Loiseau, H. Pascard, and D. Mailly, *Phys. Rev. Lett.* 78, 1791 **(1997)**.
138. Y. D. Zhang, J. I. Budnick, W. A. Hines, C. L. Chien, and J. Q. Xiao, *Appl. Phys. Lett.* 72, 2053 **(1998)**.

REVIEW
Delivered by Ingenta to: Purdue Libraries : 132.163.4.102 Mon, 15 Aug 2008 21:09:39
AMERICAN SCIENTIFIC PUBLISHERS

139. R. H. Victora, *Phys. Rev. Lett.* 63, 457 **(1989)**.
140. R. Alben, J. J. Becker, and M. C. Chi, *J. Appl. Phys.* 49, 1653 **(1978)**.
141. G. Herzer, *Scr. Metall. Mater.* 33, 1741 **(1995)**.
142. A. Hernando, P. Marín, M. Vázquez, J. M. Barandiarán, and G. Herzer, *Phys. Rev. B* 58, 366 **(1998)**.
143. A. Michels, R. N. Viswanath, J. G. Barker, R. Birringer, and J. Weissmüller, *Phys. Rev. Lett.* 91, 267204 **(2003)**.
144. J. F. Löffler, H.-B. Braun, and W. Wagner, *Phys. Rev. Lett.* 85, 1990 **(2000)**.
145. F. Luis, J. M. Torres, L. M. García, J. Bartolomé, J. Stankiewicz, F. Petroff, F. Fettar, J.-L. Maurice, and A. Vaurés, *Phys. Rev. B* 65, 094409 **(2002)**.
146. D. Fiorani (ed.), Surface Effects in Magnetic Nanoparticles, Kluwer Academic Publishers **(2005)**, XIV, p. 300, 148 illus., Hardcover.
147. U. Gradmann and K. H. J. Buschow (eds.), Handbook of Magnetism Materials, Elsevier, Amsterdam **(1993)**, Vol. 7, Chap. 1.
148. R. D. Zysler, H. Romero, C. A. Ramos, E. De Biasi, and D. Fiorani, *J. Magn. Magn. Mater.* 266, 233 **(2003)**.
149. S. Sako, K. Ohshima, M. Sakai, and S. Bandow, *Surf. Rev. Lett.* 3, 109 **(1996)**.
150. S. Sako and K. Ohshima, *J. Phys. Soc. Jpn.* 64, 944 **(1995)**.
151. J. Merikosky, J. Timonen, M. Mannien, and P. Jena, *Phys. Rev. Lett.* 66, 938 **(1991)**.
152. H. Kachkachi, A. Ezzir, M. Noguèz, and E. Tronc, *Eur. Phys. J. B* 14, 681 **(2000)**.
153. J. P. Chen, C. M. Soresen, K. J. Klabunde, and G. C. Hadjipanayis, *Phys. Rev. B* 51, 11527 **(1995)**.
154. R. H. Kodama, A. E. Berkovitz, E. J. Mc Niff, Jr., and S. Foner, *Phys. Rev. Lett.* 77, 394 **(1996)**.
155. R. H. Kodama and A. E. Berkovitz, *Phys. Rev. B* 59, 6321 **(1999)**.
156. E. Winkler, R. D. Zysler, M. Vasquez Mansilla, and D. Fiorani, *Phys. Rev. B* 72, 132409 **(2005)**.

Received: 14 September 2006. Accepted: 14 June 2007.

Delivered by Ingenta to:
Boulder Labs Library
IP : 132.163.130.249
Mon, 11 Aug 2008 19:50:43